NATIONAL ADVISORY COMMITTEE FOR AERONAUTICS

TECHNICAL NOTE

No. 1722

PREDICTION OF THE EFFECTS OF PROPELLER OPERATION ON THE STATIC LONGITUDINAL STABILITY OF SINGLE-ENGINE TRACTOR MONOPLANES WITH FLAPS RETRACTED

By Joseph Weil and William C. Sleeman, Jr.

Langley Aeronautical Laboratory
Langley Field, Va.

Washington
October 1948

NATIONAL ADVISORY COMMITTEE FOR AERONAUTICS

TECHNICAL NOTE NO. 1722

PREDICTION OF THE EFFECTS OF PROPELLER OPERATION ON THE STATIC LONGITUDINAL STABILITY OF SINGLE-ENGINE TRACTOR MONOPLANES WITH FLAPS RETRACTED

By Joseph Weil and William C. Sleeman, Jr.

SUMMARY

The effects of propeller operation on the static longitudinal stability of single-engine tractor monoplanes are analyzed, and a simple method is presented for computing power-on pitching-moment curves for flap-retracted flight conditions. The methods evolved are based on the results of powered-model wind-tunnel investigations of 28 model configurations. Correlation curves are presented from which the effects of power on the downwash over the tail and the stabilizer effectiveness can be rapidly predicted. The procedures developed enable prediction of power-on longitudinal stability characteristics that are generally in very good agreement with experiment.

INTRODUCTION

The prediction of the effects of propeller operation on the static longitudinal stability and control characteristics of single-engine tractor airplanes has been the object of many investigations. Successful methods have been developed for estimating the direct propeller forces and the effects of slipstream on the wing-fuselage characteristics (references 1 to 4). Attempts to predict the complex changes in flow at the tail plane, however, have been somewhat less successful, primarily because many of the early researchers were hindered by insufficient experimental data for developing methods of proven general applicability.

During the war years an appreciable amount of experimental data pertaining to power effects on static longitudinal stability was obtained. An analysis of these data suggested the possibilities of a semiempirical approach to the problem of determining the effects of power on the tail contribution to stability. This approach has been followed in the present paper and a simple, rapid method for determining the effects of power on the tail contribution is presented. Use of the procedures developed permit the accurate prediction of power-on longitudinal stability and trim characteristics. No analysis has been made for the flap-deflected condition.

SYMBOLS

C_L	lift coefficient
C_m	pitching-moment coefficient
$c_{m_{ac}}$	average section pitching-moment coefficient about aerodynamic center for wing section immersed in slipstream
T_c	thrust coefficient $\left(\frac{\text{Thrust}}{\rho V^2 D^2}\right)$
T_{c_A}	thrust coefficient corresponding to power-off lift coefficient
ΔT_c	increment of thrust coefficient from power-off condition to a specified power condition
V	airspeed, feet per second
ρ	air density, slugs per cubic foot
S'	propeller disk area, square feet
S	area of wing or tail, square feet
b	span of wing or tail, feet
b'	propeller-blade section chord, feet
D	propeller diameter, feet
R	propeller radius, feet
r	radius to any propeller blade element, feet
$\bar{c}_w$	wing mean aerodynamic chord, feet
c_r	wing root chord at plane of symmetry, feet
c_b	wing chord at break for wings having composite plan forms, feet
c_t	wing chord at theoretical tip, feet
c_w	wing chord at spanwise station 0.50R or 0.75R from airplane center line, feet

A	wing aspect ratio
λ	wing taper ratio (c_t/c_r for wings having linear taper)
z	distance from reference center of gravity to thrust line measured perpendicular to thrust line (positive when c.g. is above thrust line), feet
l_p	distance from reference center of gravity to propeller center line measured parallel to thrust line, feet
l_t	distance from reference center of gravity to elevator hinge line, feet
d_t	distance from elevator hinge line to thrust line measured perpendicular to thrust line (positive when elevator hinge line is above thrust line), feet
α	angle of attack, radians unless otherwise denoted
β	propeller blade angle, degrees
i_t	stabilizer setting with respect to thrust line (positive when trailing edge is down), degrees
δ_e	elevator setting with respect to chord line of stabilizer (positive when trailing edge is down), degrees
ϵ	effective angle of downwash at horizontal tail, degrees
ϵ'	increment of power-off downwash at horizontal tail from zero lift downwash, degrees
$\epsilon_{L=0}$	power-off downwash angle at zero lift
$C_{Y'_\psi}$	derivative of propeller normal-force coefficient with respect to angle of inclination of thrust line in radians
$C_{Y'_{\psi_o}}$	value of $C_{Y'_\psi}$ for $T_c = 0$
S.F.F.	abbreviation for propeller side-force factor $\left(\frac{10^5}{32}\int_{0.2}^{1.0} \frac{b'}{D} \sin\left(\beta - \beta_{0.75R} + 25^\circ\right) d\frac{r}{R}\right)$
f	ratio of $C_{Y'_\psi}$ to $C_{Y'_{\psi_o}}$
f_o	ratio of $C_{Y'_\psi}$ for power-off value of T_c to $C_{Y'_{\psi_o}}$

F	empirical taper-ratio factor
R_t	ratio of power-on stabilizer effectiveness $\left(\frac{dC_m}{di_t}\right)_p$ to power-off stabilizer effectiveness $\left(\frac{dC_m}{di_t}\right)_o$
R_e	ratio of power-on elevator effectiveness $\left(\frac{dC_m}{d\delta_e}\right)_p$ to power-off elevator effectiveness $\left(\frac{dC_m}{d\delta_e}\right)_o$
Δ	change in a quantity due to power

Subscripts:

T	thrust line
e	elevator
t	horizontal tail
P	propeller
p	power on
o	power off
w	wing
wf	wing-fuselage combination
i	immersed in slipstream

BASIS OF ANALYSIS

The method of computing power-on pitching moments which is outlined herein is based on the assumption that power-off (propeller-off or windmilling) pitching-moment and lift data are available for at least two stabilizer settings and with the tail off. The accuracy with which the effects of power on the tail contribution to stability can be predicted is dependent on the basic power-off data, and when possible these data should be obtained from wind-tunnel tests.

When power-off wind-tunnel data are not available for use in preliminary design, the power-off characteristics may be estimated by use of references 5 to 11. The wing mean aerodynamic chord and aerodynamic center may be found by the method presented in reference 5. The lift-curve slope, angle of zero lift, and pitching-moment characteristics of the wing may be computed by use of references 6 and 7. The effect of the fuselage on the wing-fuselage pitching moments may be determined by Multhopp's method (references 8 and 9). A satisfactory approximation of the horizontal-tail effectiveness can be obtained when the isolated horizontal-tail effectiveness found by the method of reference 10 is multiplied by a factor of 0.9.

The variation of power-off downwash with angle of attack computed by use of the charts of reference 11 generally was found to agree fairly well with the variation of effective downwash with angle of attack obtained from wind-tunnel data when the computed downwash was multiplied by a factor of 0.9 for all conditions for averaging downwash across the tail span instead of the factors obtained from figure 21 of reference 11. The absolute angle of downwash computed by use of the charts of reference 11 had to be adjusted, of course, so that this angle would agree with the test downwash angle at zero lift. This adjustment was necessary since an appreciable amount of effective downwash was found to exist at zero lift chiefly as a direct result of local flow angularity at the tail caused by the flow pattern over the rear of the fuselage. This downwash is often difficult to predict accurately. Neglecting the downwash at zero lift, however, will not affect the basic longitudinal stability or the estimated power effects but will alter only the trim characteristics.

The experimental data upon which the results of this paper are based were obtained from wind-tunnel investigations of powered models of specific military airplanes. In figure 1 two views of each model and in table I the geometric characteristics of the configurations used are presented. Most of the models were tested in the Langley 7- by 10-foot tunnel at an effective Reynolds number of approximately 1.6×10^6. The power-off data were obtained with the propeller windmilling at a value of $T_c \approx -0.015$. Models 25 to 27 were tested in the Ames 7- by 10-foot tunnel at an effective Reynolds number of approximately 2.0×10^6. The basic power-off data used for these latter models were obtained with the propeller removed.

METHOD OF ANALYSIS

In the following discussion the individual component effects contributing to the over-all power-on static longitudinal stability are treated separately and approximate formulas are developed for estimating these effects.

Effect of Power on the Wing-Fuselage Characteristics

Direct propeller effects.- The increment of lift coefficient contributed by the direct propeller thrust due to the inclination of the thrust line (the lift component of the normal force which is usually small being neglected) is given by the following equation:

$$\Delta C_{L_P} = T_c \frac{2D^2}{S_w} \sin \alpha_T \tag{1}$$

The increment of pitching-moment coefficient contributed by the propeller as a direct result of the thrust and the normal forces is given by the following equation, which was developed from equation (5) of reference 1:

$$\Delta C_{m_P} = \frac{S'}{S_w}\left[\frac{8}{\pi}\frac{z}{\bar{c}_w}\Delta T_c + (f - f_o)C_{Y',\psi_o}\left(\alpha_T + \alpha_w \frac{d\epsilon}{d\alpha}\right)\frac{l_P}{\bar{c}_w}\right] \tag{2}$$

where α_w is the absolute angle of attack (radians) of wing from zero lift. Figures needed for use in equation (2) have been reproduced from reference 1 and are presented as figures 2 to 5. The term $f - f_o$, obtained from figure 2, is the difference in $C_{Y',\psi}/C_{Y',\psi_o}$ for power-on and power-off conditions. It should be noted, however, that $f_o = 0$ when power-off data are obtained with the propeller removed. The term C_{Y',ψ_o}, obtained from figures 3 and 4, is the normal-force derivative; figures 3(a) and 4(a) are for low-speed propellers having thick, cambered blades; figures 3(b) and 4(b) are for high-speed propellers having thin, wide blades; plan-form curves of propellers on which figures 3 and 4 are based may be found in figure 4 of reference 1. The term $d\epsilon/d\alpha$, the upwash factor, is obtained from figure 5.

Slipstream effect on wing-fuselage characteristics.- The method most widely used for computing the increase in wing lift due to the slipstream is given by Smelt and Davies in reference 3. This method requires several successive approximations, however, to obtain final power-on lift coefficients when T_c varies with C_L. An approximate formula has been developed which is shorter than that of reference 3 and which requires only a single estimation to obtain the final value of ΔC_{L_w}; thus an appreciable amount of computing time is saved. This equation is given by

$$\Delta C_{L_w} = 0.57 T_{c_A} C_{L_o} \frac{c_w}{\bar{c}_w} \frac{D^2}{S_w} \tag{3}$$

where c_w is the wing chord at spanwise station 0.75R from airplane center line for wings behind single rotating propellers or 0.50R for wings behind dual rotating propellers.

Very close agreement is shown between the values given by equation (3) and two approximations computed by the method of reference 3. (See fig. 6.) Somewhat less agreement is shown between the values given by equation (3) and test data (fig. 7). The scatter shown can be attributed to the idealized assumptions in the theory of reference 3 and the experimental inaccuracy of the test data. The effect of propeller tilt on ΔC_{L_w} is small as shown by reference 12, the data of model 24, and other unpublished data and may be neglected for tilt angles up to at least 5°.

The effect of the slipstream on wing pitching moments is small in some cases, but it may be relatively large in others. This pitching-moment increment is obtained from equation (5) of reference 2 and is given as follows:

$$\Delta C_{m_w} = c_{m_{ac}} \frac{c_{w_i}}{\bar{c}_w} \frac{b_{w_i} c_{w_i}}{S_w} \frac{8}{\pi} T_c + \left[\left(\frac{dC_m}{dC_L}\right)_{wf}\right]_o \Delta C_{L_w} \tag{4}$$

where

$c_{m_{ac}}$ average section pitching-moment coefficient about aerodynamic center for part of wing immersed in slipstream

b_{w_i} span of wing immersed in slipstream (taken as 0.9D)

c_{w_i} average chord of wing immersed in slipstream

$\left[\left(\frac{dC_m}{dC_L}\right)_{wf}\right]_o$ rate of change of wing-fuselage pitching-moment coefficient with lift coefficient (propeller off)

Effect of Power on the Tail Contribution to Stability

Change in downwash angle due to power.— The downwash at the tail plane with the propeller removed is known to be chiefly dependent upon the wing lift coefficient and the location of the tail with respect to the wing vortex system. When a propeller is added in front of the wing, many complex changes in flow occur which affect the downwash over the tail; but the chief effects are probably caused by the increase in wing lift coefficient and altered wing span load distribution brought about by the passage of the propeller slipstream over the wing. Although appreciable downwash may exist behind an isolated propeller at an angle of attack, large changes in the inclination of the thrust line (at constant wing angle of attack) were found (reference 13) to cause practically no change in effective downwash at the tail when a wing was located between the propeller and the tail. With the foregoing discussion as a basis the following simplified semiempirical approach was used to derive a parameter with which to correlate experimental downwash changes due to power.

Downwash angles were computed for several models for which extensive constant thrust data were available. When $\Delta\epsilon$ was plotted against T_c at various angles of attack, $\Delta\epsilon$ was found to be a function of both T_c and α. This relationship seemed logical for the increase in wing lift with power, and any resultant span-load changes would also depend on T_c and α; however, ϵ' was believed to be a better factor than α for use in the correlation inasmuch as ϵ' usually varies linearly with α up to fairly high lift coefficients and also depends on tail location. The assumption was made that a tail well out of the power-off maximum downwash field would also be favorably located in the power-on downwash field for configurations within the range of geometry of the models presented.

Model 17, which has an untapered wing, showed a considerably larger increase in ϵ with the application of power than either model 13 or model 16, which had identical tail and fuselage geometry but rather highly tapered wing plan forms. The power-off downwash angles were considerably less for the model with the untapered plan form, but the downwash for all three wing plan forms could be accurately computed from the charts of reference 11. With power, however, the downwash angles for models 13, 16, and 17 were much closer to the same value.

According to lifting-line theory the downwash behind a wing of arbitrary plan form in a uniform air stream (at a given tail location and lift coefficient) depends only on the span load distribution along the wing. Wing taper ratio has a significant bearing on the span load distribution and hence the downwash at the tail, the downwash increasing with wing taper. The data of reference 14 show that the slipstream alters the span load distribution by increasing the loading over the inboard part of the wing. Since the greatest change in downwash with taper occurs for values of λ near unity, a wing of rectangular plan form

might be expected to be more susceptible to this induced taper effect and show the largest change of downwash angle with power. The experimental results of models 13 and 17 agree with the foregoing assumptions; however, further substantiation would be desirable.

An empirical factor F (fig. 8) which is a function of wing taper ratio was derived from the data of models 13, 16, 17, and other models with similar tail geometry to account for induced taper effects. The taper ratio for wings of composite plan form may be satisfactorily estimated by use of an equivalent root chord c_r', as shown in the sketch in figure 8.

A plot of the parameter $(\Delta T_c)_\epsilon' F$ against the experimental $\Delta\epsilon$ obtained from stabilizer and tail-off wind-tunnel data for 28 model configurations is shown in figure 9(a). The dash-line curves in the figure indicate the approximate accuracy of determining downwash angles from complete-model wind-tunnel data. The correlation of test points indicates that the parameters selected account for the first-order effects of power rather well. The solid-line curve indicates the suggested curve for use in design and is reproduced in figure 9(b) without experimental test data.

Note that figure 9(b) indicates no change in $\Delta\epsilon$ attributable to the tilt of the propeller thrust axis. The data of model 24 and other unpublished data show that changes in $\Delta\epsilon$ with tilt are small and rather inconsistent and the effect of tilt (at least for tilt angles up to 5°) can be satisfactorily estimated from considerations of direct thrust effects and changes in stabilizer effectiveness.

Change in stabilizer effectiveness with power.— The slipstream is considerably distorted in the region of the horizontal tail, and idealized theoretical methods which assume a cylindrical slipstream at the tail do not always produce a satisfactory estimate of the change in dynamic pressure at the tail associated with the application of power. As was true for the downwash correlation, a semiempirical approach was followed to derive a method for predicting the change in stabilizer effectiveness with power.

The ratio of power-on to power-off stabilizer effectiveness R_t was assumed to be directly proportional to ΔT_c and the ratio of the propeller diameter to tail span. A maximum value of R_t was also assumed to be attained for the tail located on the thrust line with a linear decline in R_t occurring until a value of unity is reached for a tail location 1 propeller diameter above or below the thrust line. Experimental points were plotted against the parameters suggested by the foregoing assumptions (fig. 10) and the following relationship was obtained:

$$R_t = 1.0 + 2.1\left[(\Delta T_c)\,\frac{D}{b_t}\left(1 - \frac{|d_t|}{D}\right)\right] \qquad (5)$$

The dash-line curves in figure 10 indicate the approximate limits of accuracy of determining R_t from wind-tunnel test data, and essentially all the test points fall within these limits.

Change in elevator effectiveness with power.- Inasmuch as most airplanes utilize the elevator for longitudinal control, it is apparent that the increase in elevator effectiveness $\frac{dC_m}{d\delta_e}$ with power will influence the determination of the final power-on stability and trim characteristics of the airplane. An analysis was made to determine the possibility of correlating R_e in a manner similar to the foregoing correlation of R_t. The results of this analysis were less consistent than the results obtained with the correlation of R_t, probably for the most part because of appreciable scale effects on some of the model elevator data and the reduced accuracy possible in setting the elevator-deflection angles. For full-span elevators when estimated power-on elevator data are desired, however, it may be assumed in most instances that $R_e = R_t$.

Computation of Power-on Lift and Pitching-Moment Coefficients

Power-on wing-fuselage lift coefficient.- The final power-on wing-fuselage lift coefficient is given by

$$\left(C_{L_{wf}}\right)_p = \left(C_{L_{wf}}\right)_o + \left(\Delta C_{L_p}\right)_2 + \Delta C_{L_w} \tag{6}$$

In order to arrive at a value of $\left(C_{L_{wf}}\right)_p$ from equation (6), the following procedure is recommended for conditions where T_c varies with C_L: The increment of the wing lift coefficient due to power is first evaluated by equation (3). The second-approximation of the increment of lift coefficient contributed by the propeller $\left(\Delta C_{L_p}\right)_2$ is obtained by computing a first approximation $\left(\Delta C_{L_p}\right)_1$ by equation (1) with values of T_c corresponding to $\left(C_{L_{wf}}\right)_o + \Delta C_{L_w}$; the second approximation is then obtained by use of equation (1) with values of T_c corresponding to $\left(C_{L_{wf}}\right)_o + \Delta C_{L_w} + \left(\Delta C_{L_p}\right)_1$. The second approximation will usually give a value of $\left(C_{L_{wf}}\right)_p$ such that further approximation will be unnecessary.

Power-on wing-fuselage pitching-moment coefficients.- The final power-on wing-fuselage pitching-moment coefficient is given by

$$\left(C_{m_{wf}}\right)_p = \left(C_{m_{wf}}\right)_o + \Delta C_{m_p} + \Delta C_{m_w} \tag{7}$$

The terms ΔC_{m_p} and ΔC_{m_w} are found from equations (2) and (4), with values of T_c based on $\left(C_{L_{wf}}\right)_p$ as given by equation (6).

Power-on tail pitching-moment coefficient.- The computation of the power-on tail pitching-moment coefficient merely consists of adding the increments produced by the altered downwash at the tail and increased tail effectiveness to $\left(C_{m_t}\right)_o$; this coefficient is given by

$$\left(C_{m_t}\right)_p = R_t\left(C_{m_t}\right)_o - \Delta\epsilon \left[R_t\left(\frac{dC_m}{di_t}\right)_o\right] \tag{8}$$

Power-on complete-model pitching-moment and lift coefficients.- The final power-on complete-model pitching-moment coefficient is given by adding equation (7) and equation (8) as follows:

$$C_{m_p} = \left(C_{m_{wf}}\right)_p + \left(C_{m_t}\right)_p \tag{9}$$

Inasmuch as

$$\left(C_{L_t}\right)_p = -\frac{\left(C_{m_t}\right)_p}{l_t/\bar{c}_w} \tag{10}$$

the final power-on complete-model lift coefficient is given by adding equation (6) and equation (10) as follows:

$$C_{L_p} = \left(C_{L_{wf}}\right)_p + \left(C_{L_t}\right)_p \tag{11}$$

Illustrative Example

A detailed step-by-step procedure for computing power-on lift coefficients and pitching-moment coefficients for model 21 is presented in table II. The sample calculations in table II illustrate the use of the equations presented in this paper and give the pertinent constants and column headings in a convenient form for general application to design. The data from which these estimations were made and the final computed power-on characteristics are presented in figures 11 and 12. Model 21 was chosen as an example because, although the individual component effects of power were not small, the design variables were such that the adverse effects were counteracted by the favorable effects and thus a very small over-all change in stability with power resulted. Calculations for models 13 and 15 were also made to show that the change of power effects attributable to raising the horizontal tail and increasing its area can be accurately predicted. The basic data and estimations of power effects for these models are presented in figures 11, 13, and 14.

The computed results for all three models show very good agreement with the test results.

DISCUSSION

The range of the most pertinent geometric variables for the models used in this paper are presented in table III. The correlation curves of figures 6, 9, and 10 are believed to be valid at least between the limits given in table III. No data on powered models with appreciable wing sweep were available; consequently, the effect of sweep could not be included in the correlating parameters.

Wind-tunnel data on personal-type airplanes were not available for use in the correlations, and the applicability of the curves in figures 9 and 10 to this type of design is dependent on a number of factors. Although the models used in the present correlation represent highly powered fighter-type airplanes, the correlation curves were found to be valid for medium power conditions on the fighter-type airplane models also. An estimate of the variation of T_c with C_L for several typical single-engine personal-type airplanes showed that the thrust coefficients for maximum rated power for these airplanes fell in the range of thrust coefficients for the medium power conditions on the fighter-type airplanes.

The range of wing vertical positions relative to the slipstream and the ratio of the slipstream diameter to the wing span might be expected to be considerably different for military and personal-type airplanes, and these differences could have a significant bearing on the magnitude of the power effects.

All models presented herein have a wing location that placed the wing well within the slipstream. The increment of wing lift due to the slipstream derived from the data of reference 15 does not vary appreciably with wing height for wing positions 0.3 propeller diameter above and below the thrust line when the propeller is more than 0.3 root chord ahead of the wing leading edge. The range of wing vertical positions for the models presented herein is 0.165 and 0.176 propeller diameters above and below the thrust line, respectively, and the propellers are more than 0.3 root chord ahead of the wing leading edge; thus the range falls within the limits of wing and propeller locations where computed values of ΔC_{L_w} would be expected to be valid.

Generally, the diameter of the propeller relative to the wing span is smaller for personal-type airplanes than for fighter-type airplanes. Model 24 has a relative propeller diameter approximately the same as for the personal-type airplanes considered, but the other models used in the correlations had larger relative propeller diameters. No definite conclusions can be made regarding the effect of relative propeller size because of insufficient data. In most instances, the methods outlined in the present paper should be satisfactory for computing the first-order effects of propeller operation on personal-type single-engine tractor airplanes.

OPTIMUM DESIGN CONSIDERATIONS

The design configuration usually considered optimum when satisfactory handling qualities of airplanes are considered is that which exhibits no change in longitudinal stability characteristics upon the application of power. Many design parameters affect the longitudinal stability both adversely and favorably, and defining a definite method by which to design an airplane with no power effects is difficult. Often considerations other than aerodynamic determine the final geometry of a design. In view of this fact and the rapidity with which the power effects of a specific configuration can be computed by the method of the present paper, each proposed design should be examined for power effects, and an optimum configuration (minimum power effects) should be attained by a process of rational modification to the original design.

Langley Aeronautical Laboratory
National Advisory Committee for Aeronautics
Langley Field, Va., July 13, 1948

REFERENCES

1. Ribner, Herbert S.: Notes on the Propeller and Slipstream in Relation to Stability. NACA ARR No. L4I12a, 1944.

2. Pass, H. R.: Wind-Tunnel Study of the Effects of Propeller Operation and Flap Deflection on the Pitching Moments and Elevator Hinge Moments of a Single-Engine Pursuit-Type Airplane. NACA ARR, July 1942.

3. Smelt, R., and Davies, H.: Estimation of Increase in Lift Due to Slipstream. R. & M. No. 1788, British A.R.C., 1937.

4. Goett, Harry J., and Pass, H. R.: Effect of Propeller Operation on the Pitching Moments of Single-Engine Monoplanes. NACA ACR, May 1941.

5. Diehl, Walter S.: The Mean Aerodynamic Chord and the Aerodynamic Center of a Tapered Wing. NACA Rep. No. 751, 1942.

6. Abbott, Ira H., Von Doenhoff, Albert E., and Stivers, Louis S., Jr.: Summary of Airfoil Data. NACA ACR No. L5C05, 1945.

7. Anderson, Raymond F.: Determination of the Characteristics of Tapered Wings. NACA Rep. No. 572, 1936.

8. Multhopp, H.: Aerodynamics of the Fuselage. NACA TM No. 1036, 1942.

9. White, Maurice D.: Estimation of Stick-Fixed Neutral Points of Airplanes. NACA CB No. L5C01, 1945.

10. Bates, William R.: Collection and Analysis of Wind-Tunnel Data on the Characteristics of Isolated Tail Surfaces with and without End Plates. NACA TN No. 1291, 1947.

11. Silverstein, Abe, and Katzoff, S.: Design Charts for Predicting Downwash Angles and Wake Characteristics behind Plain and Flapped Wings. NACA Rep. No. 648, 1939.

12. Goett, Harry J., and Delany, Noel K.: Effect of Tilt of the Propeller Axis on the Longitudinal-Stability Characteristics of Single-Engine Airplanes. NACA Rep. No. 774, 1944.

13. Stüper, J.: Effect of Propeller Slipstream on Wing and Tail. NACA TM No. 874, 1938.

14. Robinson, Russell G., and Herrnstein, William H., Jr.: Wing-Nacelle-Propeller Interference for Wings of Various Spans. Force and Pressure-Distribution Tests. NACA Rep. No. 569, 1936.

15. Wood, Donald H.: Tests of Nacelle-Propeller Combinations in Various Positions with Reference to Wings. Part I. Thick Wing - N.A.C.A. Cowled Nacelle - Tractor Propeller. NACA Rep. No. 415, 1932.

TABLE I.- GEOMETRIC CHARACTERISTICS OF MODEL CONFIGURATIONS USED IN CORRELATIONS

Model	Symbol notation	Wing area, S_w (sq ft)	Wing span, b_w (ft)	Mean aerodynamic chord, $\bar{c}_w$ (ft)	Wing root chord, c_r (ft)	Wing break chord, c_b (ft)	Wing tip chord, c_t (ft)	NACA airfoil sections			Wing aspect ratio, A	Wing taper ratio, λ
								Wing root	Wing break	Wing tip		
1	⊙	9.40	7.51	1.310	1.683	-----	0.842	66,2-216	----------	66,2-216	6.00	0.50
2	⊡	9.40	7.51	1.310	1.683	-----	.842	66,2-216	----------	66,2-216	6.00	.50
3	◇	9.40	7.51	1.310	1.683	-----	.842	66,2-216	----------	66,2-216	6.00	.50
4	△	9.40	7.51	1.310	1.683	-----	.842	66,2-216	----------	66,2-216	6.00	.50
5	◁	9.40	7.51	1.310	1.683	-----	.842	66,2-216	----------	66,2-216	6.00	.50
6	▷	9.40	7.51	1.310	1.683	-----	.842	66,2-216	----------	66,2-216	6.00	.50
7	◺	9.40	7.51	1.310	1.683	-----	.842	66,2-216	----------	66,2-216	6.00	.50
8	◿	9.40	7.51	1.310	1.683	-----	.842	66,2-216	----------	66,2-216	6.00	.50
9	◿	9.40	7.51	1.310	1.683	-----	.842	66,2-216	----------	66,2-216	6.00	.50
10	⊙	9.40	7.51	1.310	1.683	-----	.842	66,2-216	----------	66,2-216	6.00	.50
11	⊙	9.28	7.14	1.352	1.750	-----	.875	23015.6	----------	23009	5.50	.50
12	⊙	10.19	7.50	1.428	1.638	1.638	.819	65(318)-118.5	----------	66,2-216	5.52	.41
13	▽	6.34	6.25	1.021	1.693	1.021	.494	23014.7	23016	23008	6.16	.32
14	◇	6.34	6.25	1.021	1.693	1.021	.494	23014.7	23016	23008	6.16	.32
15	⊡	6.34	6.25	1.021	1.693	1.021	.494	23014.7	23016	23008	6.16	.32
16	⊙	6.34	6.25	[a]	1.693	1.021	.494	23014.7	23016	23008 (approx.)	6.16	.32
17	◁	6.34	6.25	1.021	1.021	1.021	1.021	23016	23016	23009	6.16	1.00
18	▽	7.26	6.25	[a]	1.693	1.021	1.021	23014.7	23016	23009	5.38	.77
19	▷	5.18	5.961	.969	1.431	1.042	.378	66,2-118	66(2x15)-117.63	66(2x15)-116	6.8	.275
20	⊙	9.76	7.10	1.460	1.931	-----	.858	23016.5 (modified)	----------	23009	5.17	.445
21	◺	8.55	7.30	1.220	1.375	1.375	.688	2416	2416	4412	6.83	.41
22	⊙	9.44	7.458	1.360	1.800	-----	.800	2215	----------	2209	5.91	.445
23	◿	9.44	7.458	1.360	1.800	-----	.800	2215	----------	2209	5.91	.445
24	▷	8.57	7.50	1.198	1.542	-----	.771	23018 (modified)	----------	23012 (modified)	6.56	.500
[b]24a	◺	8.57	7.50	1.198	1.542	-----	.771	23018 (modified)	----------	23012 (modified)	6.56	.500
25	◸	13.18	8.438	1.627	2.094	-----	1.047	6-series	----------	6-series	5.40	.500
26	◸	13.18	8.438	1.627	2.094	-----	1.047	6-series	----------	6-series	5.40	.500
27	◸	13.76	8.99	1.605	2.094	-----	.977	----------	----------	----------	5.87	.469

[a] Pitching-moment coefficients based on same S_w and model pivot location as for models 13, 14, 15, and 17.

[b] Model 24a is the same as model 24 except that the thrust line is tilted 3° down about a point 4.0 inches aft of propeller disk.

TABLE I.- GEOMETRIC CHARACTERISTICS OF MODEL CONFIGURATIONS USED IN CORRELATIONS - Concluded

Model	Center of gravity to propeller center line, l_p (ft)	Center of gravity to elevator hinge line, l_t (ft)	Center of gravity to thrust line, z (ft)	Center of gravity location (percent $\bar{c}_w$)	Propeller diameter, D (ft)	Number of propeller blades	Propeller side-force factor, S.F.F.	Horizontal tail area, S_t (sq ft)	Horizontal tail span, b_t (ft)	Tail height above thrust line, d_t (ft)
1	1.527	2.629	-0.095	28.2	2.270	3	98.2	1.436	2.723	0.433
2	1.527	2.687	-.095	28.2	2.270	3	98.2	2.150	3.333	.433
3	1.527	2.743	-.095	28.2	2.270	3	98.2	2.988	3.930	.433
4	1.527	3.573	-.095	28.2	2.270	3	98.2	1.436	2.723	.433
5	1.527	3.631	-.095	28.2	2.270	3	98.2	2.150	3.333	.433
6	1.527	3.687	-.095	28.2	2.270	3	98.2	2.988	3.930	.433
7	1.527	5.249	-.095	28.2	2.270	3	98.2	1.436	2.723	.433
8	1.527	5.307	-.095	28.2	2.270	3	98.2	2.150	3.333	.433
9	1.527	5.362	-.095	28.2	2.270	3	98.2	2.988	3.930	.433
10	1.527	3.631	-.095	28.2	2.270	3	98.2	1.886	2.936	.433
11	1.454	3.508	-.130	27.3	2.175	3	70.3	2.16	3.083	-0.092
12	1.454	3.508	-.130	28.8	2.175	3	70.3	2.16	3.083	-0.092
13	1.317	2.993	-.035	22.0	1.817	6	82.3	1.240	2.229	.250
14	1.317	2.993	-.035	22.0	1.817	6	82.3	1.455	2.839	.250
15	1.317	2.993	-.035	22.0	1.817	6	82.3	1.455	2.839	.750
16	1.317	2.993	-.035	a	1.817	6	82.3	1.240	2.229	.250
17	1.317	2.993	-.035	22.0	1.817	6	82.3	1.240	2.229	.250
18	1.317	2.993	-.035	a	1.817	6	82.3	1.240	2.229	.250
19	1.152	2.722	-.094	26.7	1.555	6	81.55	1.061	1.923	.185
20	1.41	3.443	-.053	24.64	2.517	3	91.7	2.06	3.141	0
21	1.680	3.3	-.103	23.6	2.035	4	69.8	1.80	2.775	.625
22	1.37	3.720	-.058	26.7	2.000	3	75.8	1.92	2.560	.719
23	1.37	3.720	-.058	26.7	2.000	3	75.8	1.92	2.560	.719
24	1.756	2.963	.072	25.0	1.625	4	150.3	2.14	3.021	.344
[b]24a	1.756	2.963	.003	25.0	1.625	4	150.3	2.14	3.021	.115
25	2.161	4.20	.016	25.0	2.521	4	-----	2.82	3.333	.355
26	2.213	4.20	.016	25.0	2.375	4	-----	2.82	3.333	.355
27	2.3	4.27	.005	27.4	2.375	4	----	3.042	3.722	.398

[a]Pitching-moment coefficients based on same $\bar{c}_w$ and model pivot location as for models 13, 14, 15, and 17.

[b]Model 24a is the same as model 24 except that the thrust line is tilted 3° down about a point 4.0 inches aft of propeller disk.

NACA

TABLE II.- COMPUTATION OF POWER-ON PITCHING-MOMENT AND LIFT COEFFICIENTS FOR MODEL 21

[Numbers in circles refer to columns]

$\frac{c_w}{c_v} = 1.127$ $\quad \frac{S_w}{S_v} = 0.380$ $\quad$ [a]$c_{T'_{\Psi_o}} = 0.135$ $\quad c_{m_{a_o}} = -0.045$ $\quad k_{y_1} = 1.832$ ft $\quad F = 0.494$

$\frac{b_w^2}{S_v} = 0.969$ $\quad \frac{l_w}{c_v} = -0.084$ $\quad \frac{l_v}{c_v} = 1.328$ $\quad \delta_v = 1.220$ ft $\quad \epsilon_{L=0} = 1.7°$ $\quad \frac{D}{D_s}\left(1 - \frac{|d_s|}{D}\right) = 0.508$

$r_{c_o} = -0.0103$ $\quad f_o = 0.988$ $\quad$ [b]$\frac{\partial \epsilon}{\partial \alpha} = 0.16$ $\quad c_{v_1} = 1.379$ ft $\quad \lambda = 0.41$ $\quad \frac{l_t}{c_v} = 2.705$

①	②	③	④	⑤	⑥	⑦	⑧	⑨	⑩	⑪	⑫	⑬	⑭	⑮	⑯	⑰	⑱
α_p (deg)	α_T (radians)	$(C_{L_{wf}})_o$	τ_{o_λ}	ΔC_{L_w}	$(C_{L_{wf}})_o + \Delta C_{L_w}$	τ_o	$(\Delta C_{L_p})_1$	$(C_{L_{wf}})_o + \Delta C_{L_w} + (\Delta C_{L_p})_1$	τ_o	$(\Delta C_{L_p})_2$	$(C_{L_{wf}})_p$	τ_o	$\alpha\Delta\epsilon_o$	f	ΔC_{m_T} (thrust force)	ΔC_{m_n} (normal force) (o)	ΔC_{m_p}
0	0	0.220	0.041	0.0034	0.2234	0.042	0	0.2234	0.042	0	0.2234	0.042	0.0523	1.047	-0.0043	0	-0.0043
2	.0349	.372	.083	.0117	.3837	.087	.0029	.3866	.087	.0029	.3866	.087	.0973	1.082	-.0079	.0003	-.0076
4	.0698	.520	.130	.0256	.5456	.138	.0093	.5549	.142	.0096	.5552	.142	.1523	1.125	-.0124	.0008	-.0116
6	.1047	.670	.183	.0465	.7165	.200	.0203	.7368	.208	.0211	.7376	.208	.2183	1.172	-.0177	.0016	-.0161
8	.1396	.810	.236	.0725	.8825	.264	.0356	.9181	.278	.0375	.9200	.278	.2883	1.221	-.0234	.0027	-.0207
10	.1745	.951	.292	.1052	1.0562	.334	.0566	1.1124	.357	.0601	1.1163	.359	.3693	1.272	-.0300	.0041	-.0259
12	.2094	1.090	.349	.1442	1.2342	.407	.0820	1.3162	.448	.0891	1.3233	.445	.4553	1.322	-.0370	.0058	-.0312
		Full-off power-off test data.	Fig. 11. Based on ③.	④ × (0.57 $\frac{\partial C_L}{\partial \alpha_T}$ $\frac{b_w^2}{S_v}$)	③ + ⑤	Fig. 11. Based on ⑥.	⑦ × $\frac{\partial \epsilon}{\partial \alpha_T}$ sin α_T	⑥ + ⑧	Fig. 11. Based on ⑨.	⑩ × $\frac{\partial \epsilon}{\partial \alpha_T}$ sin α_T	⑥ + ⑪. Final power-on $(C_{L_{wf}})_p$	Fig. 11. Based on ⑫. Final τ_o.	⑬ − τ_{o_o}	Fig. 2. Based on ⑬.	$\frac{S_v}{S_w}\left(\frac{\partial}{\partial \alpha_T} \times ⑭\right)$	$\frac{S_v}{S_w}\left[\left(⑫ - f_o\right) C_{T'_{\Psi_o}} \frac{l_t}{c_v}\left(② + \alpha_w \frac{\partial \epsilon}{\partial \alpha}\right)\right]$	⑯ + ⑰

[a] Propeller of model 21 has blade plan form similar to the Hamilton Standard 3155-6 propeller and fig. 3(a) and 4(a) are used in determining $C_{T'_{\Psi_o}}$.

For a four-blade single-rotation propeller, $\beta_{0.75R} = 18°$, S.F.F. = 80.7, $C_{T'_{\Psi_o}} = 0.161$ (fig. 3(a)). Since S.F.F. = 65.8 for model 21, fig. 4(a) is used to correct $C_{T'_{\Psi_o}}$. Ratio of S.F.F. of desired propeller (65.8) to Hamilton Standard propeller is 0.838 (fig. 4(a)). For desired propeller, $C_{T'_{\Psi_o}} = (0.161)(0.838) = 0.135$.

[b] Obtained from fig. 5 for propeller located $1.15c_r$ ahead of $c_r/4$ and wing aspect ratio A = 6.23.

[c] $\alpha_w = \alpha_T + 0.0541$ (angles in radians).

NACA

TABLE II.- COMPUTATION OF POWER-ON PITCHING-MOMENT AND LIFT COEFFICIENTS FOR MODEL 21 - Concluded

(19)	(20)	(21)	(22)	(23)	(24)	(25)	(26)	(27)	(28)	(29)	(30)	(31)	(32)	(33)	(34)	(35)	(36)	(37)
$\left[\left(\frac{dC_m}{dC_L}\right)_{wf}\right]_o$ (d)	ΔC_{m_w}	$(C_{m_{wf}})_o$	$(C_{m_{wf}})_p$	ϵ'	$(\Delta\epsilon_o)_{\epsilon'F}$	$\Delta\epsilon$	B_t	$\left(\frac{dC_m}{di_t}\right)_o$	$(C_{m_t})_o$	$(C_{m_t})_p$	C_{m_p}	$(C_{L_t})_p$	C_{L_p}	$(C_{m_t})_o$	$(C_{m_t})_p$	C_{m_p}	$(C_{L_t})_p$	C_{L_p}
0.0809	-0.0013	-0.037	-0.0626	1.2	0.0310	0.10	1.0358	-0.0292	0.0840	0.0918	0.0292	-0.0339	0.1893	-0.0958	-0.0980	-0.1606	0.0362	0.2596
.0989	-.0023	-.042	-.0519	1.9	.0913	.27	1.1038	-.0223	.0431	.0544	.0085	-.0201	.3665	-.1328	-.1398	-.1917	.0517	.4383
.0969	-.0029	-.029	-.0435	2.7	.2031	.57	1.1625	-.0287	.0062	.0262	-.0173	-.0097	.5455	-.1661	-.1741	-.2176	.0644	.6196
.1049	-.0030	-.012	-.0311	3.4	.3666	.94	1.2329	-.0282	-.0290	-.0031	-.0342	.0011	.7387	-.1990	-.2126	-.2437	.0786	.8162
.1119	-.0025	.004	-.0192	4.2	.9982	1.43	1.3076	-.0283	-.0635	-.0301	-.0493	.0111	.9311	-.2310	-.2492	-.2684	.0921	1.0121
.1209	-.0010	.022	-.0049	4.9	.8939	2.02	1.3940	-.0280	-.0930	-.0578	-.0627	.0214	1.1377	-.2635	-.2885	-.2934	.1067	1.2230
.1279	-.0014	.040	.0102	5.4	1.2145	2.61	1.4857	-.0272	-.1330	-.0982	-.0820	.0341	1.3574	-.2950	-.3329	-.3227	.1231	1.4464
Tail off, propeller off.	$\sigma_{m_{wo}}\frac{b_{w_1}c_{w}}{S_w}\frac{S}{S_w}\times$ (13) + (19) × (5)	Tail-off power-off test data.	(18) + (20) + (21)	$\epsilon_o - \epsilon_{i_t=0}$	(14) × (23) × F	Fig. 9(b).	$1.0 + 2.1 \times$ (14) $\left[\frac{n}{b_t}\left(1 - \frac{\lvert z_t\rvert}{b_t}\right)\right]$	Tail-on power-off test data.	Power-off test data, tail off and $i_t = 0°$.	(28) × (26) − (25) × (27)	(22) + (29)	$\left(\frac{dC_{L_t}}{di_t}\right)_p$ (28)	(12) + (31) $(i_t = 0°)$	Power-off test data, tail off and $i_t = 0°$.	(26) × (33) − (28) × (27)	(22) + (34) $(i_t = 0°)$	$\left(\frac{dC_{L_t}}{di_t}\right)_p$ (34)	(12) + (36) $(i_t = 0°)$

[d]Obtained by subtracting $\left(\frac{dC_{m_p}}{dC_L}\right)_{windmilling}$ as found by formula (6) of reference 1 from tail-off propeller-windmilling pitching-moment slope;

that is, $\left[\left(\frac{dC_m}{dC_L}\right)_{wf}\right]_o = \left[\left(\frac{dC_m}{dC_L}\right)_{wf}\right]_{windmilling} - 0.0151.$

NACA

TABLE III.— RANGE OF GEOMETRIC CHARACTERISTICS OF MODELS INCLUDED IN CORRELATION

Geometric parameter	Range	
	From	To
Wing aspect ratio	5.17 (model 20)	6.8 (model 19)
Wing taper ratio	0.275 (model 19)	1.00 (model 17)
$\frac{\text{Propeller diameter}}{\text{Wing span}}$	0.217 (model 24)	0.354 (model 20)
$\frac{\text{Height of tail above thrust line}}{\text{Propeller diameter}}$	0.413 (model 15)	−0.042 (model 11)
$\frac{\text{Tail span}}{\text{Wing span}}$	0.523 (model 3)	0.322 (model 19)
$\frac{\text{Tail length}}{\text{Mean aerodynamic chord}}$	2.008 (model 1)	4.09 (model 9)
$\frac{\text{Height of thrust line above wing root chord}}{\text{Propeller diameter}}$	0.165 (model 22)	−0.176 (model 23)
$\frac{\text{Distance of propeller ahead of wing root chord}}{\text{Root chord}}$	0.490 (model 13)	0.906 (model 21)

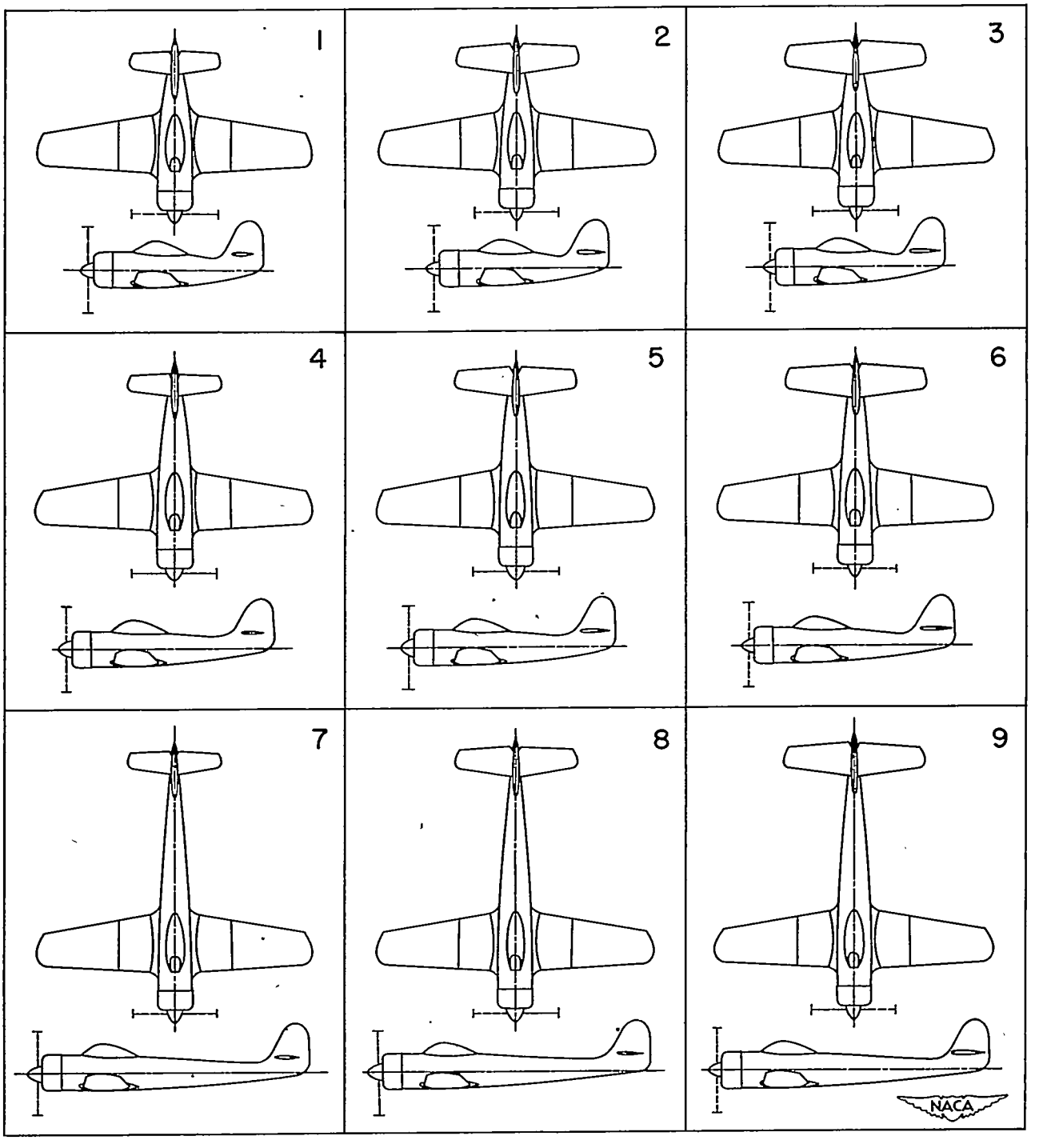

Figure 1.- Model configurations used in the correlations.

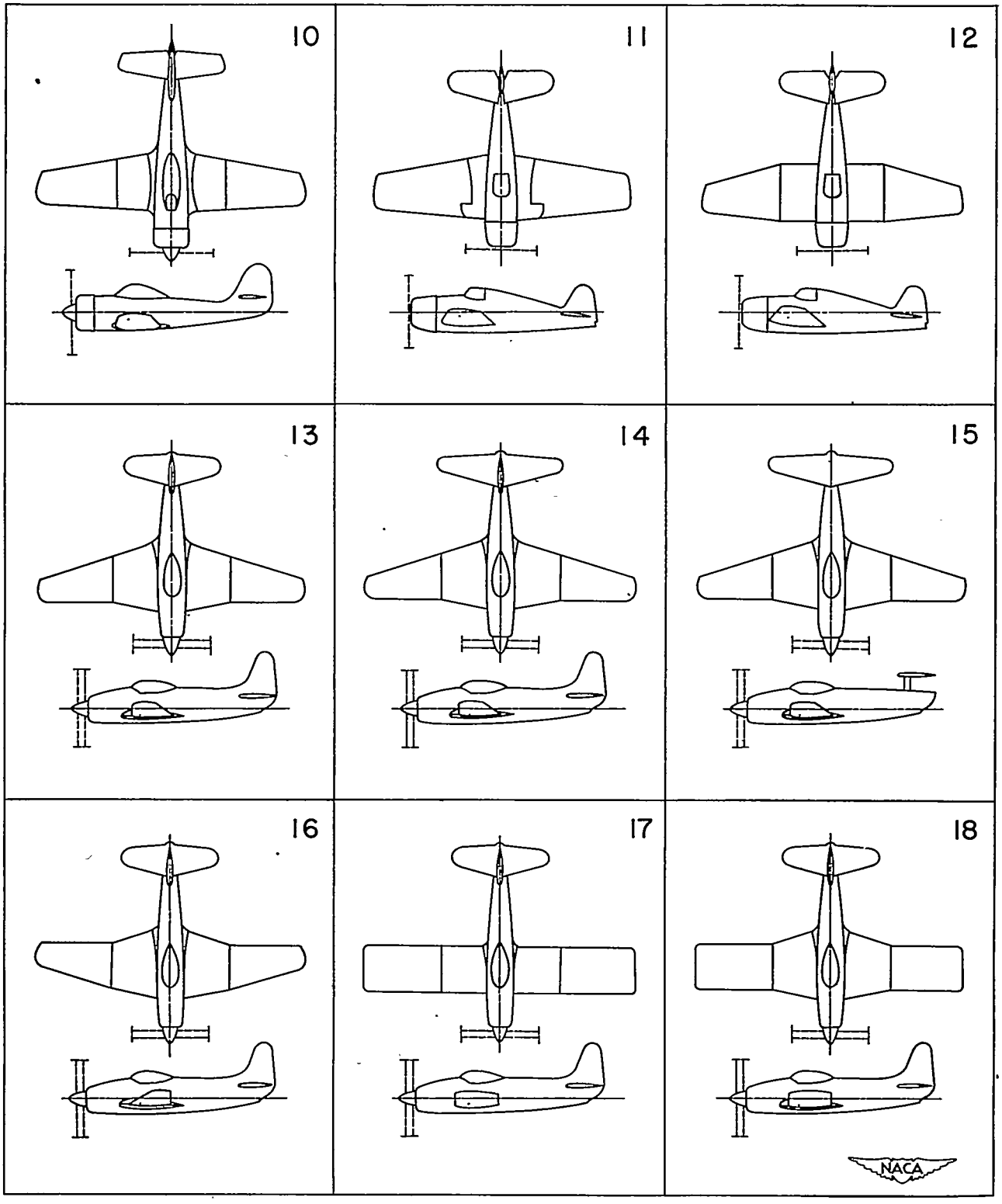

Figure 1.- Continued.

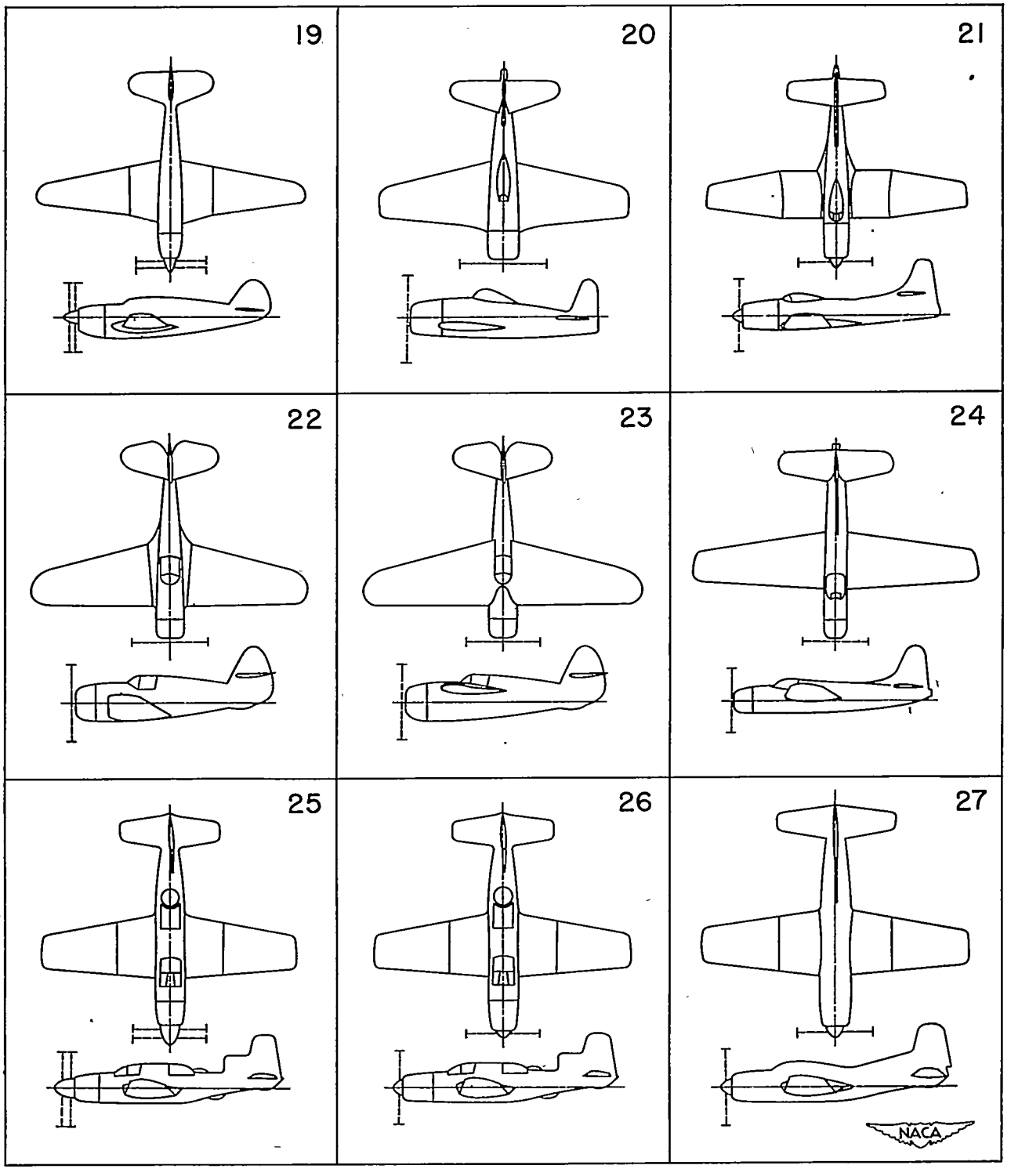

Figure 1.- Concluded.

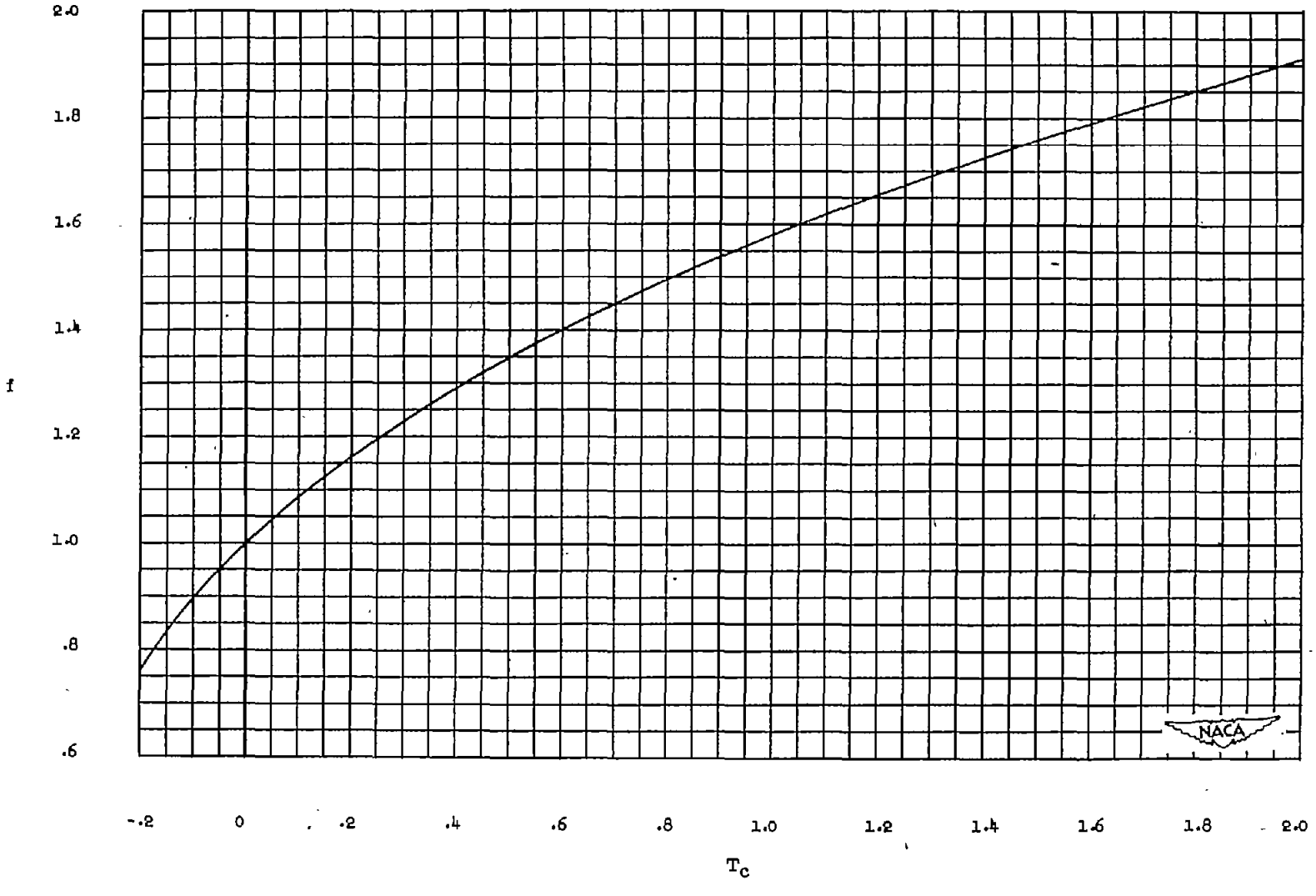

Figure 2.- Variation of f with T_c.

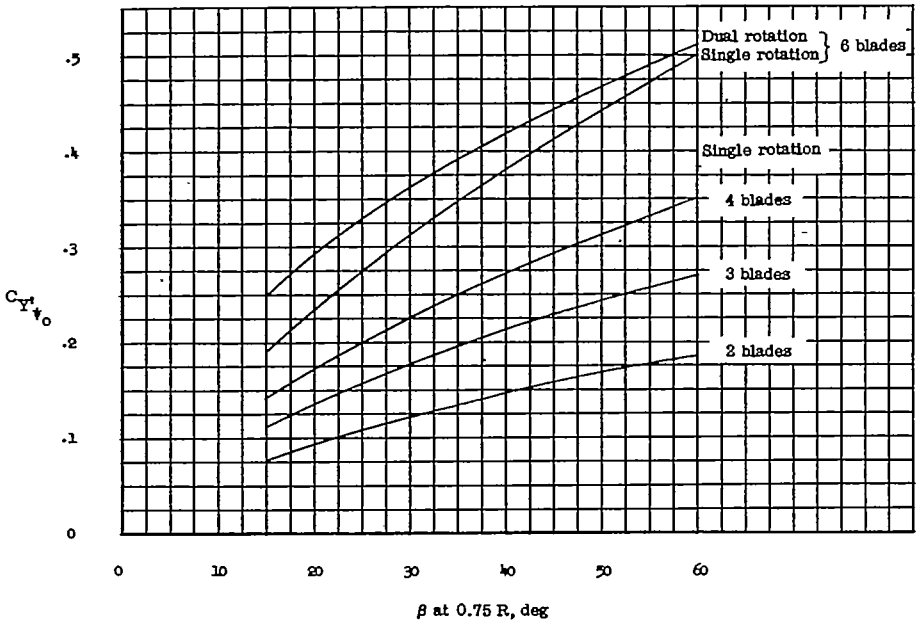

(a) Hamilton Standard 3155-6 propeller with 0.164-diameter spinner; S.F.F. = 80.7.

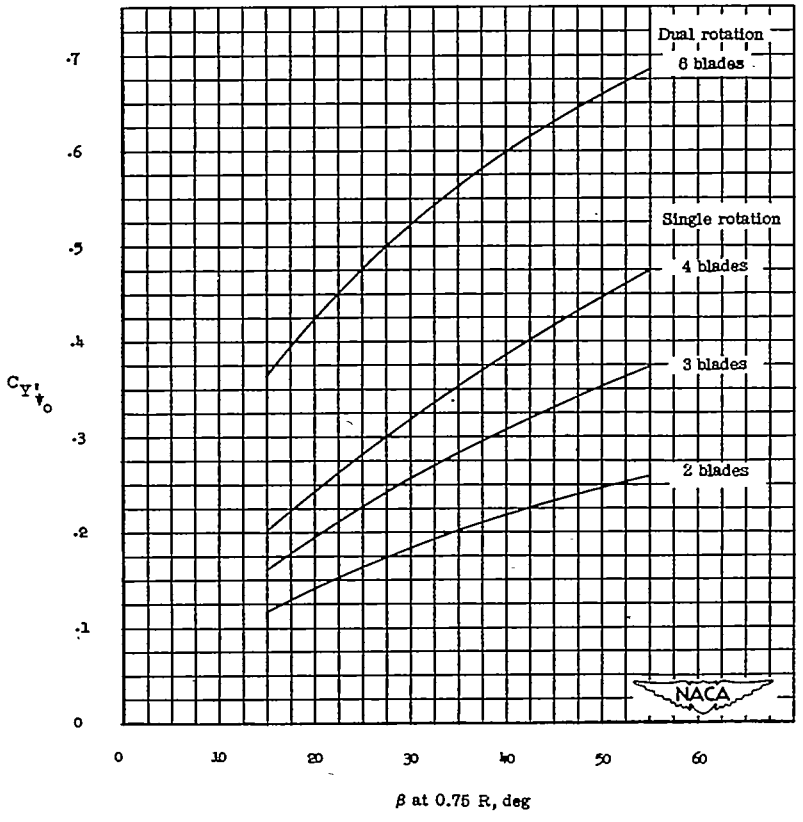

(b) NACA propeller 10-3062-045 with 0.164-diameter spinner; S.F.F. = 131.6.

Figure 3.- Variation of $C_{Y'_{\psi_o}}$ with blade angle.

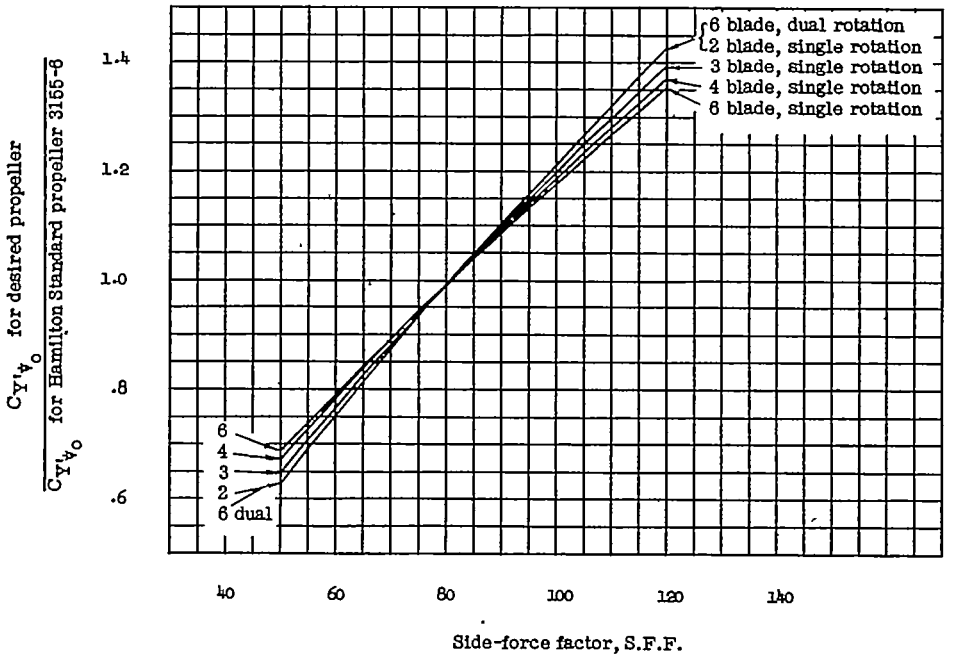

(a) Hamilton Standard propeller 3155-6; S.F.F. = 80.7.

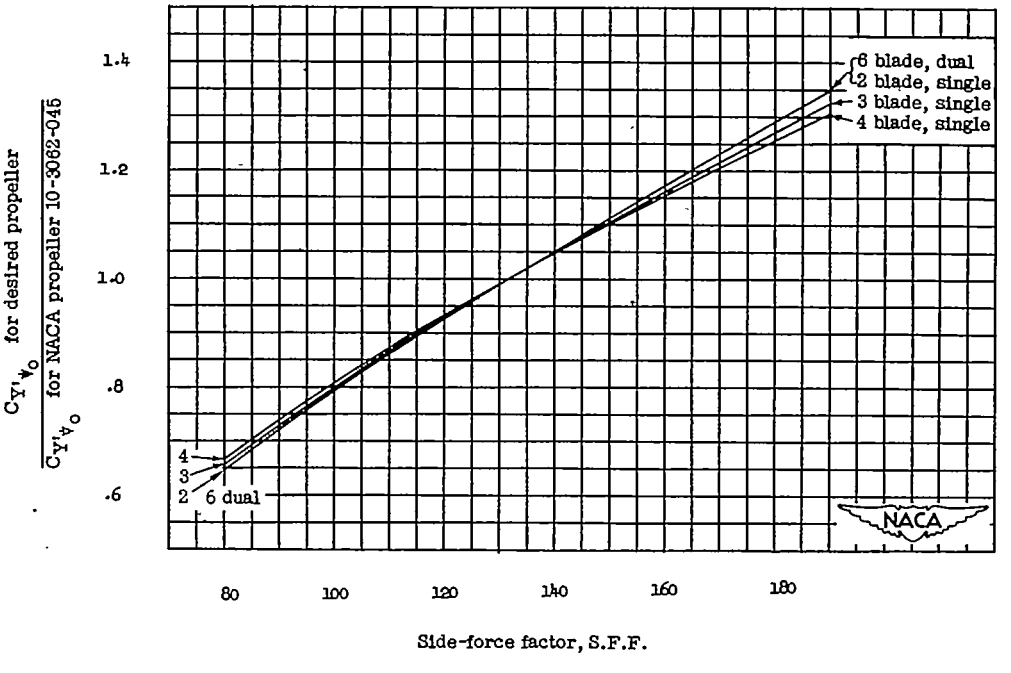

(b) NACA propeller 10-3062-045; S.F.F. = 131.6.

Figure 4.- Ratio of side-force derivatives as a function of side-force factor for desired propeller.

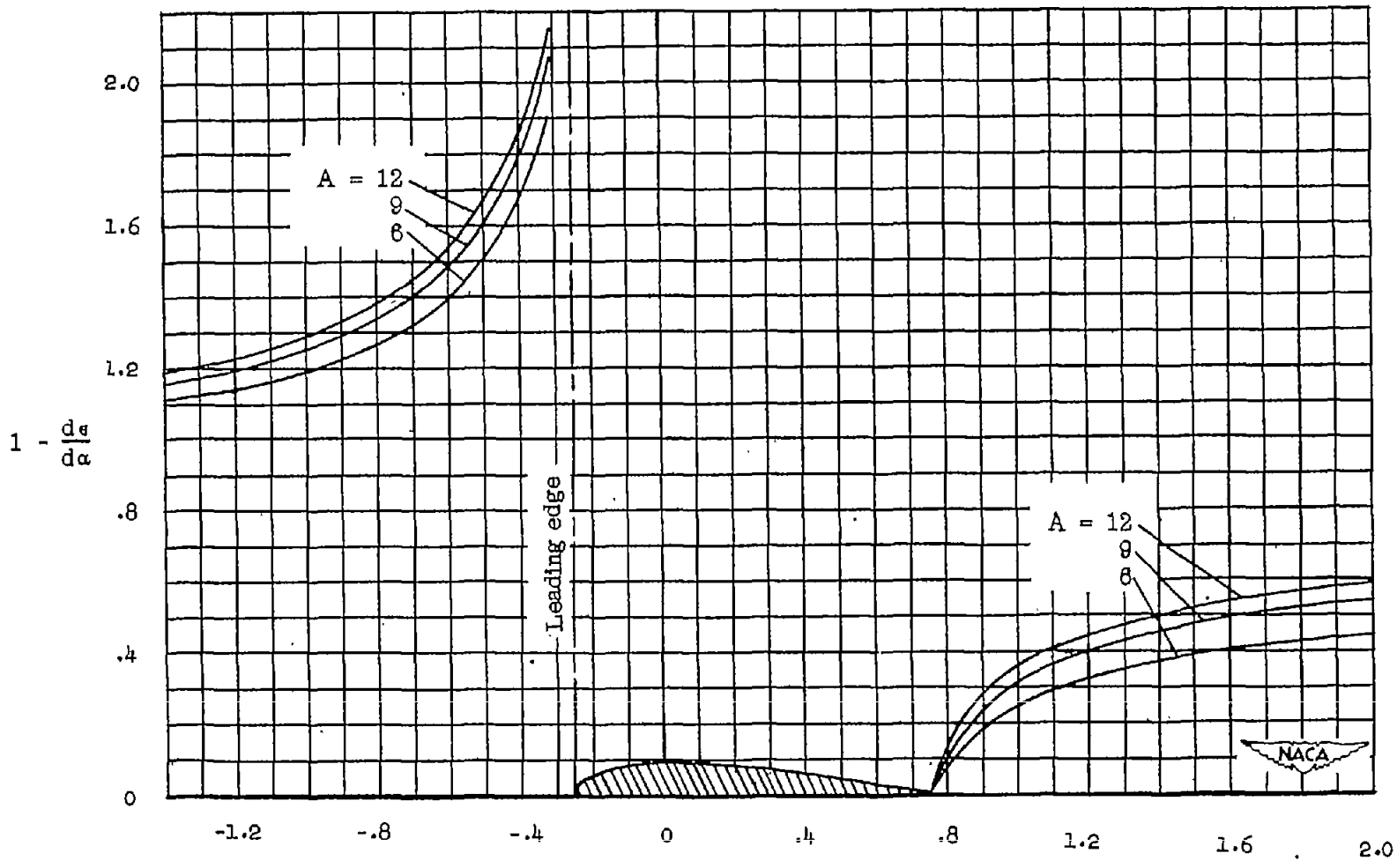

Figure 5.- Value of $1 - \frac{d\epsilon}{d\alpha}$ on longitudinal axis of elliptic wing for aspect ratios of 6, 9, and 12.

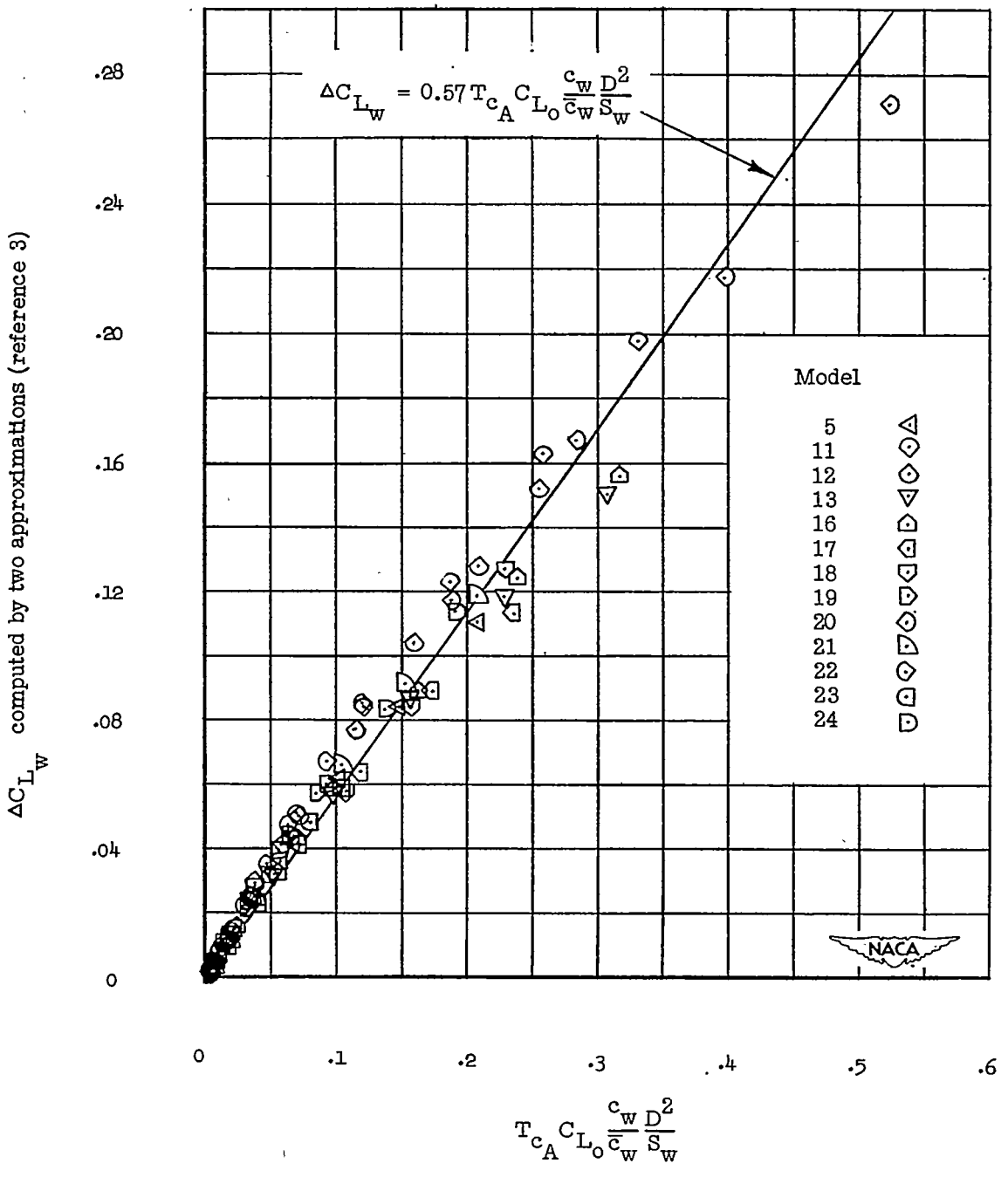

Figure 6.- Variation of the increment of wing lift attributable to the propeller slipstream as computed from two approximations by the method of reference 3 with the parameter $T_{c_A} C_{L_o} \frac{c_w}{\bar{c}_w} \frac{D^2}{S_w}$.

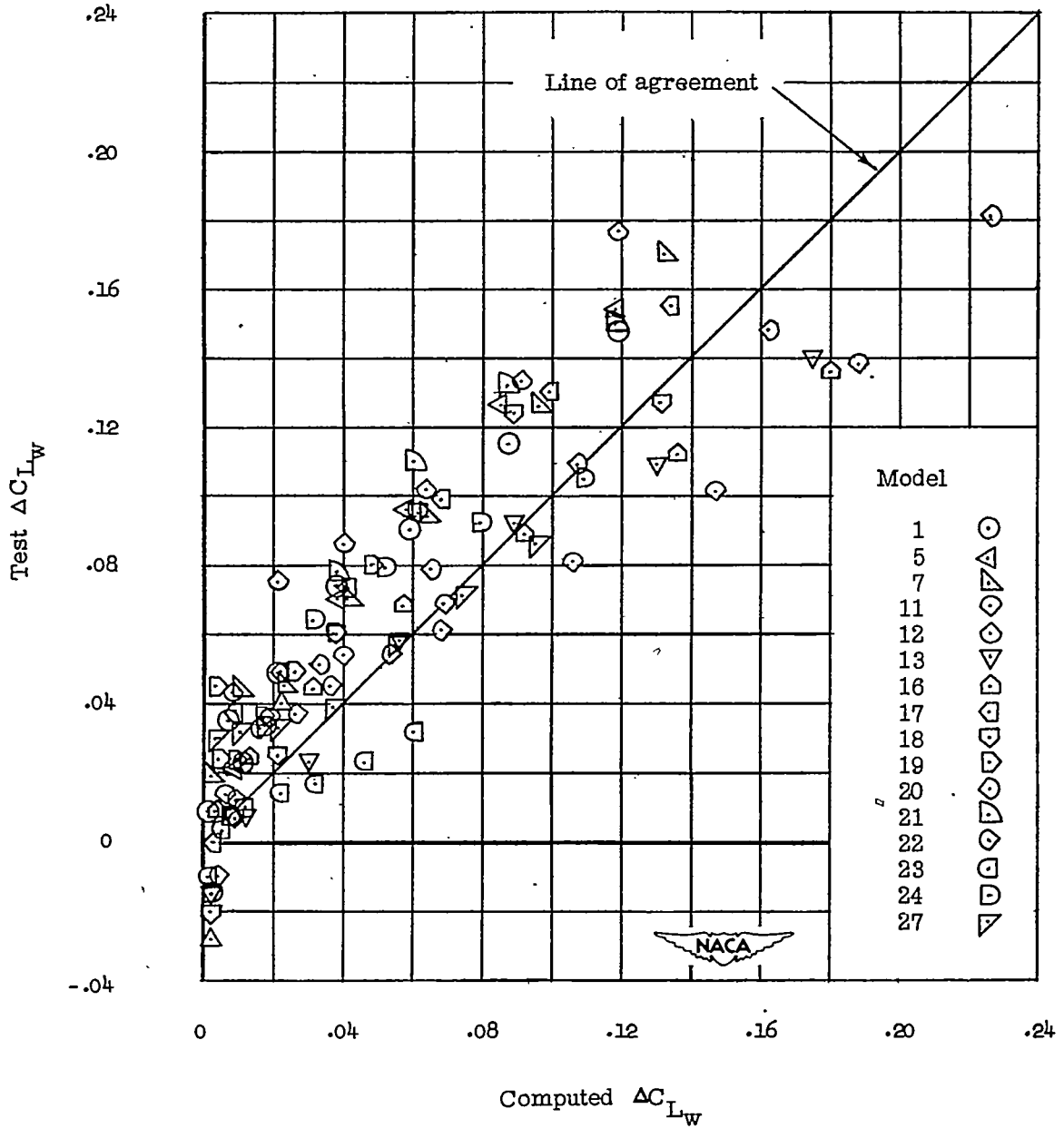

Figure 7.- Comparison of ΔC_{L_w} computed by equation 3 and obtained from test data. $\Delta C_{L_w}{}_{computed} = 0.57\, T_{c_A} C_{L_o} \frac{c_w}{\bar{c}_w} \frac{D^2}{S_w}$.

For wings having composite plan form

$$\lambda = \frac{c_t}{c_r'}$$

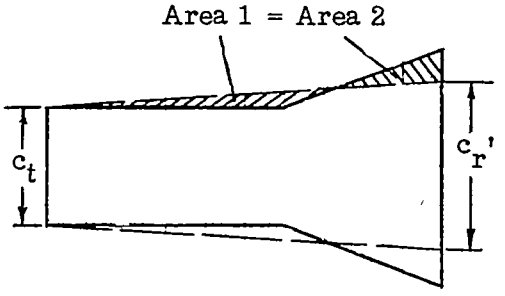

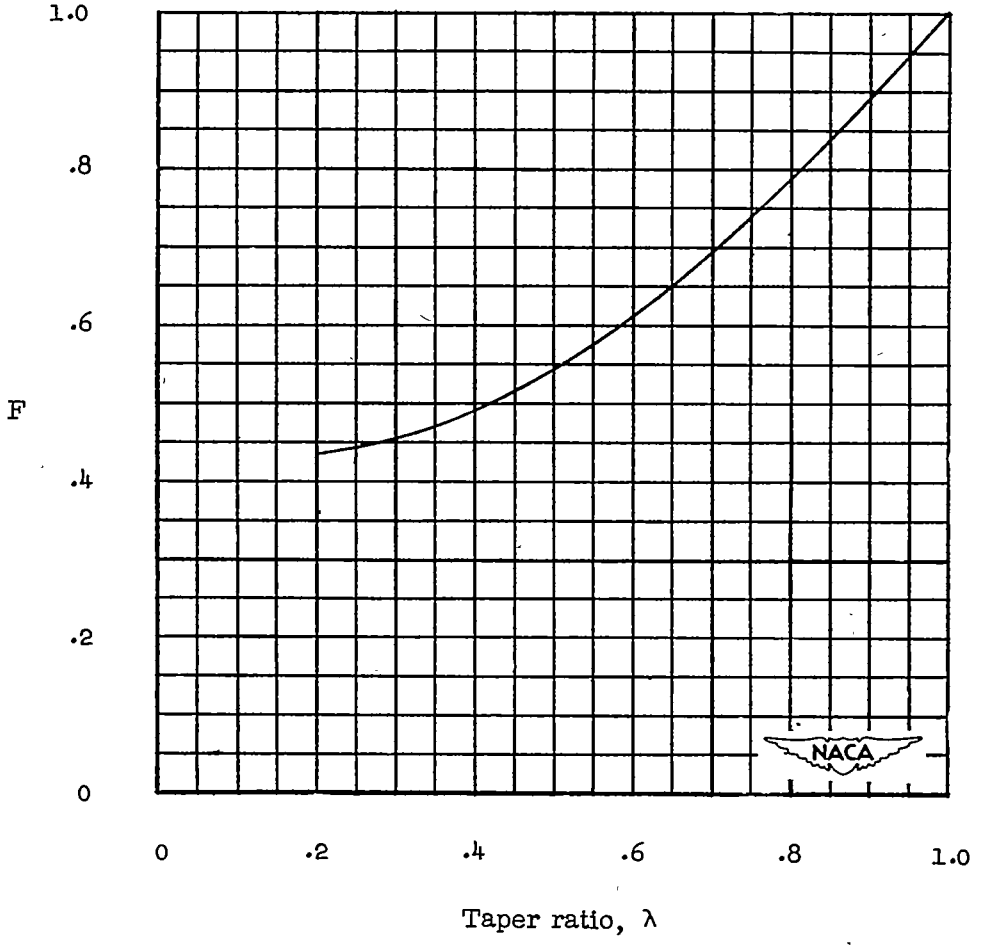

Figure 8.- Variation of empirical taper-ratio factor with taper ratio.

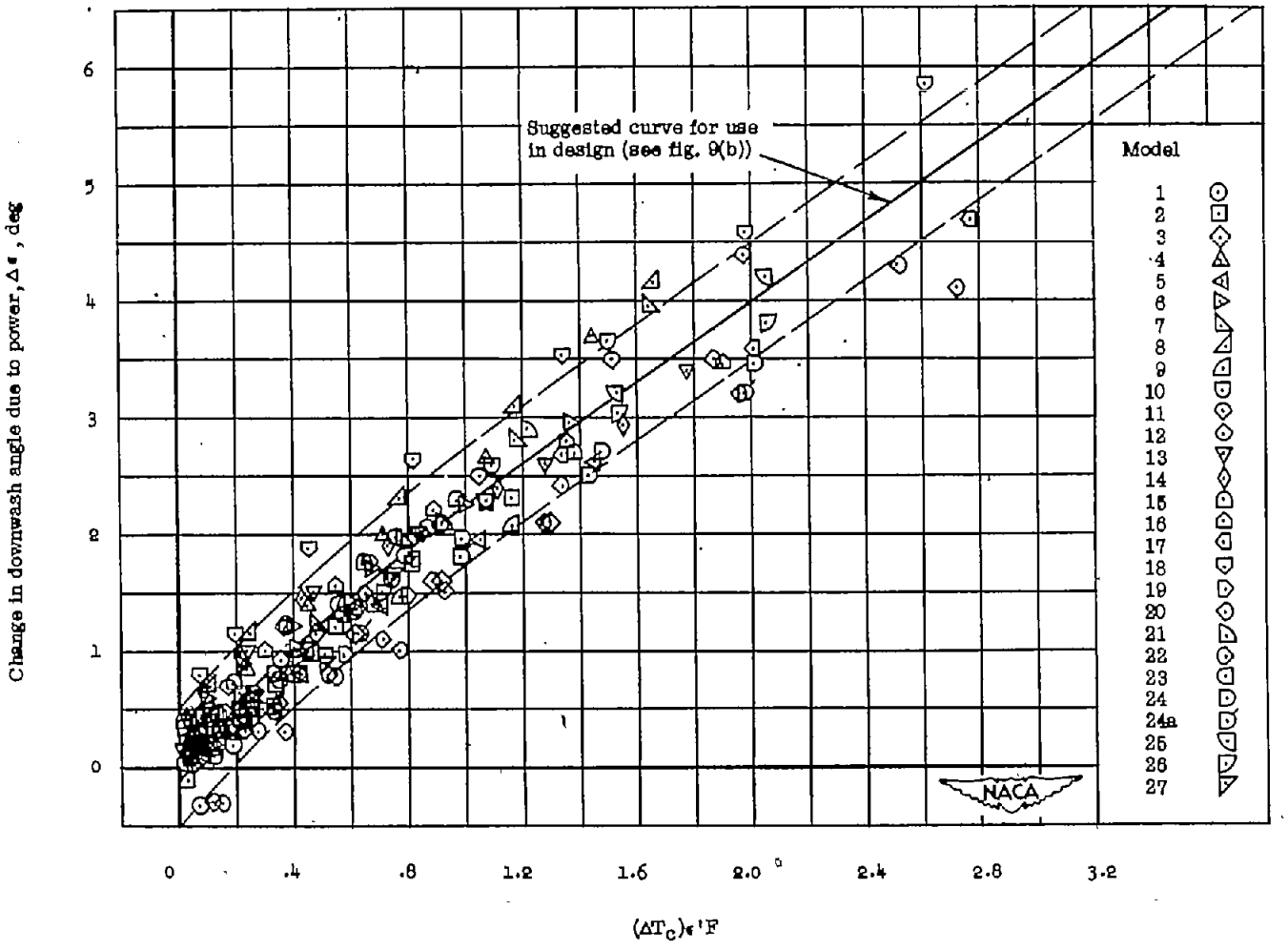

(a) Experimental data and suggested design curve.

Figure 9.- Variation of the increment of downwash angle due to power with the parameter $(\Delta T_c)\epsilon'F$.

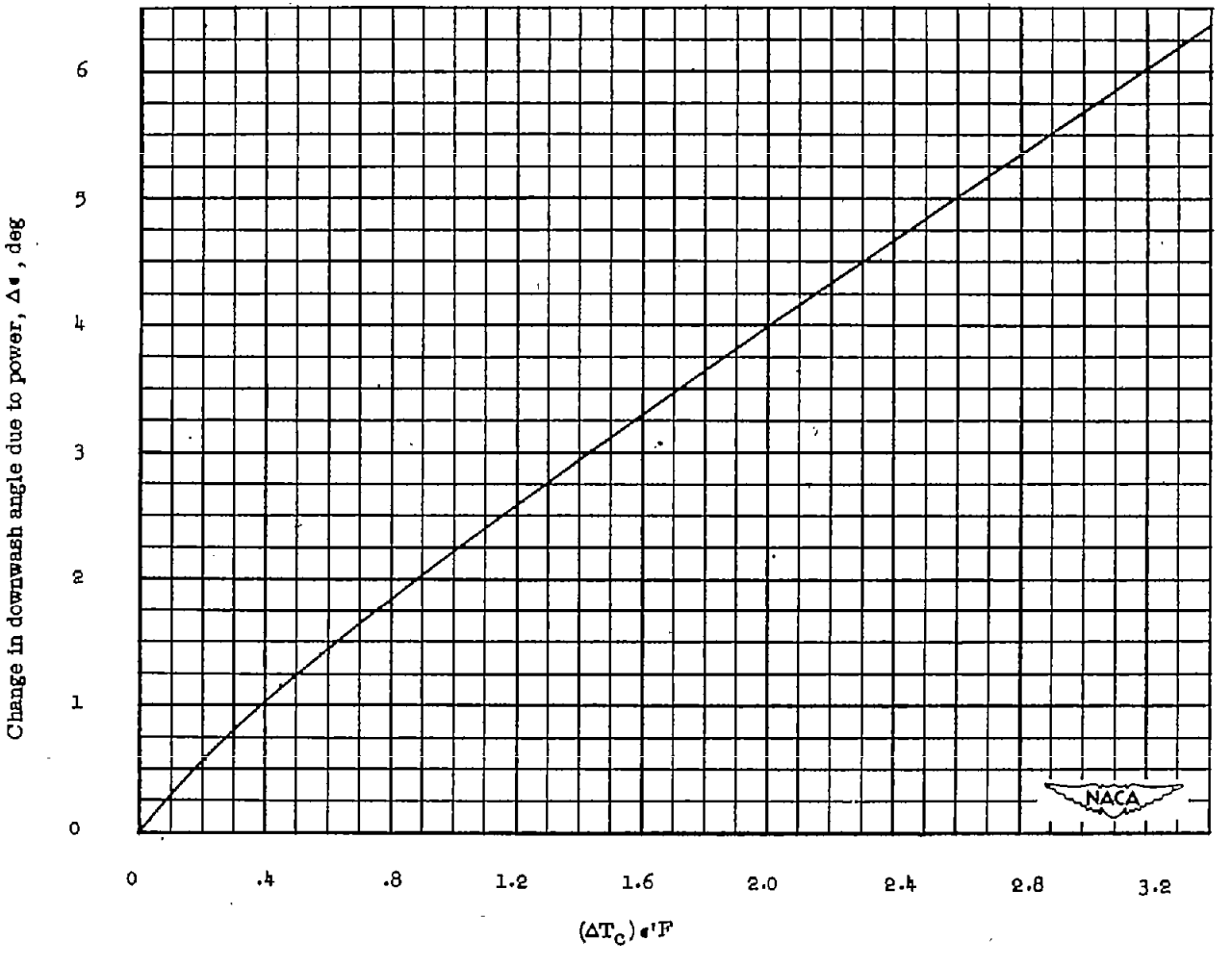

(b) Suggested design curve from figure 9(a).

Figure 9.- Concluded.

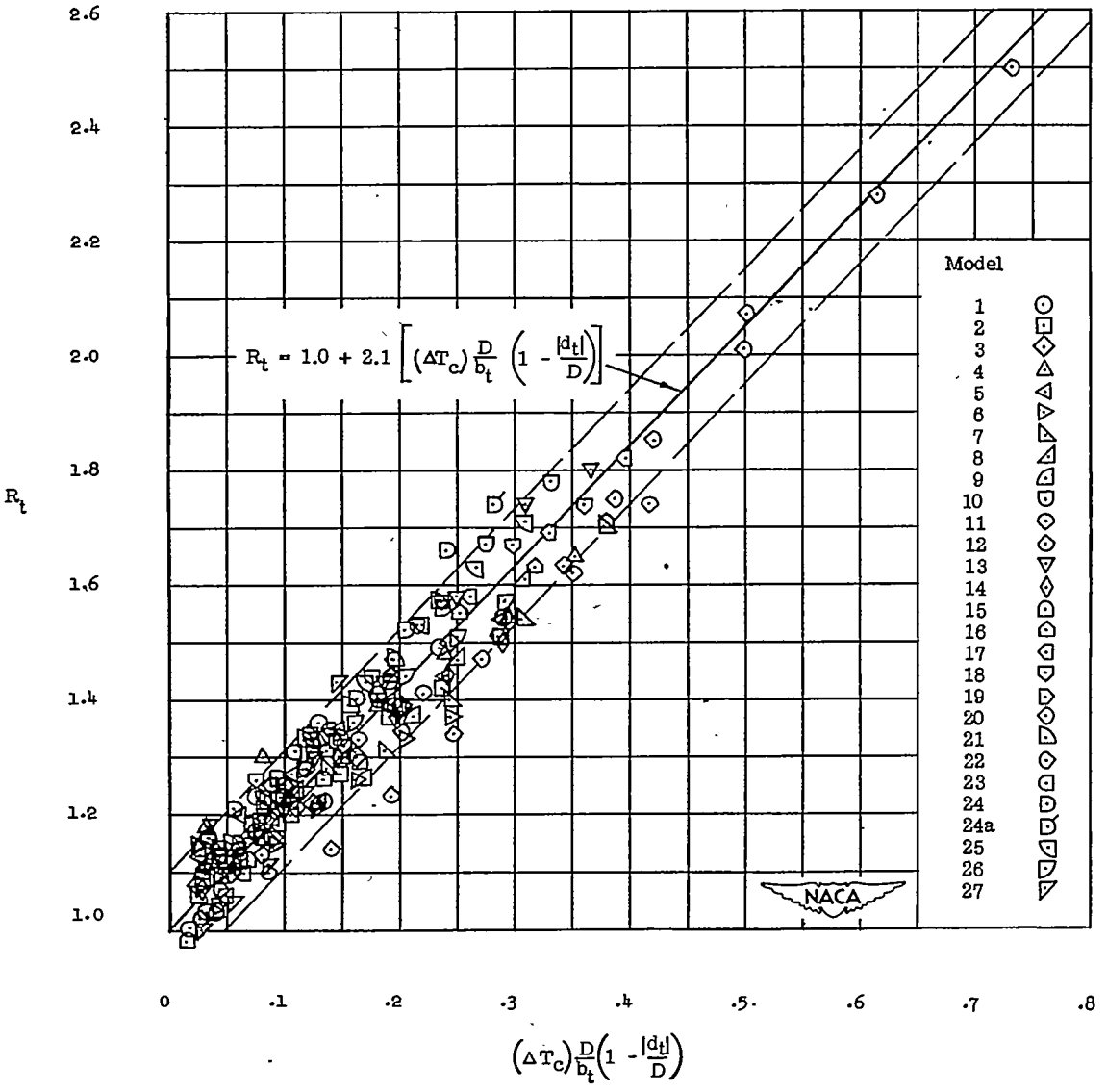

Figure 10.- Variation of experimental R_t with the parameter $(\Delta T_c)\frac{D}{b_t}\left(1 - \frac{|d_t|}{D}\right)$.

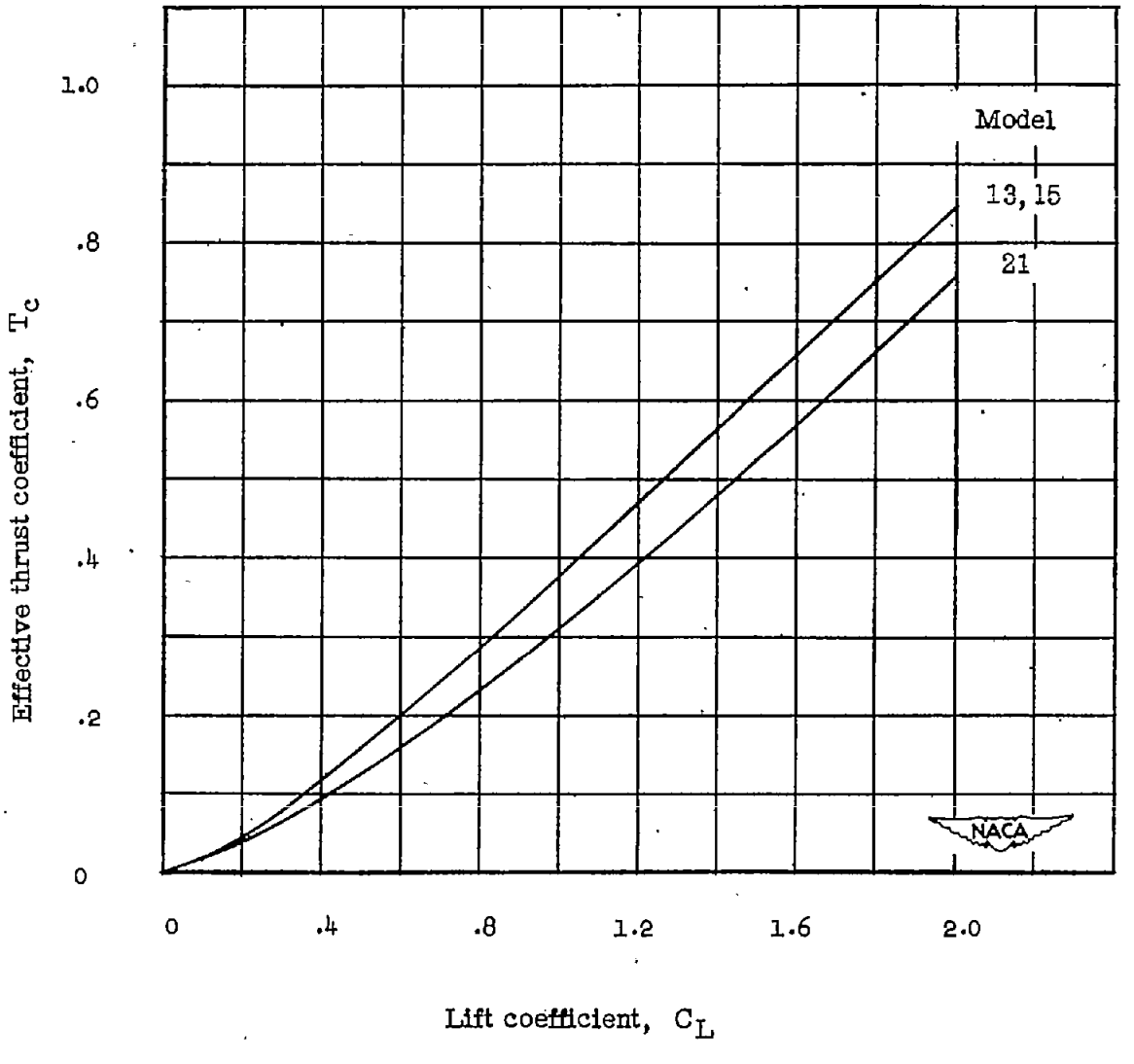

Figure 11.- Variation of constant power thrust coefficients with lift coefficient for models 13, 15, and 21.

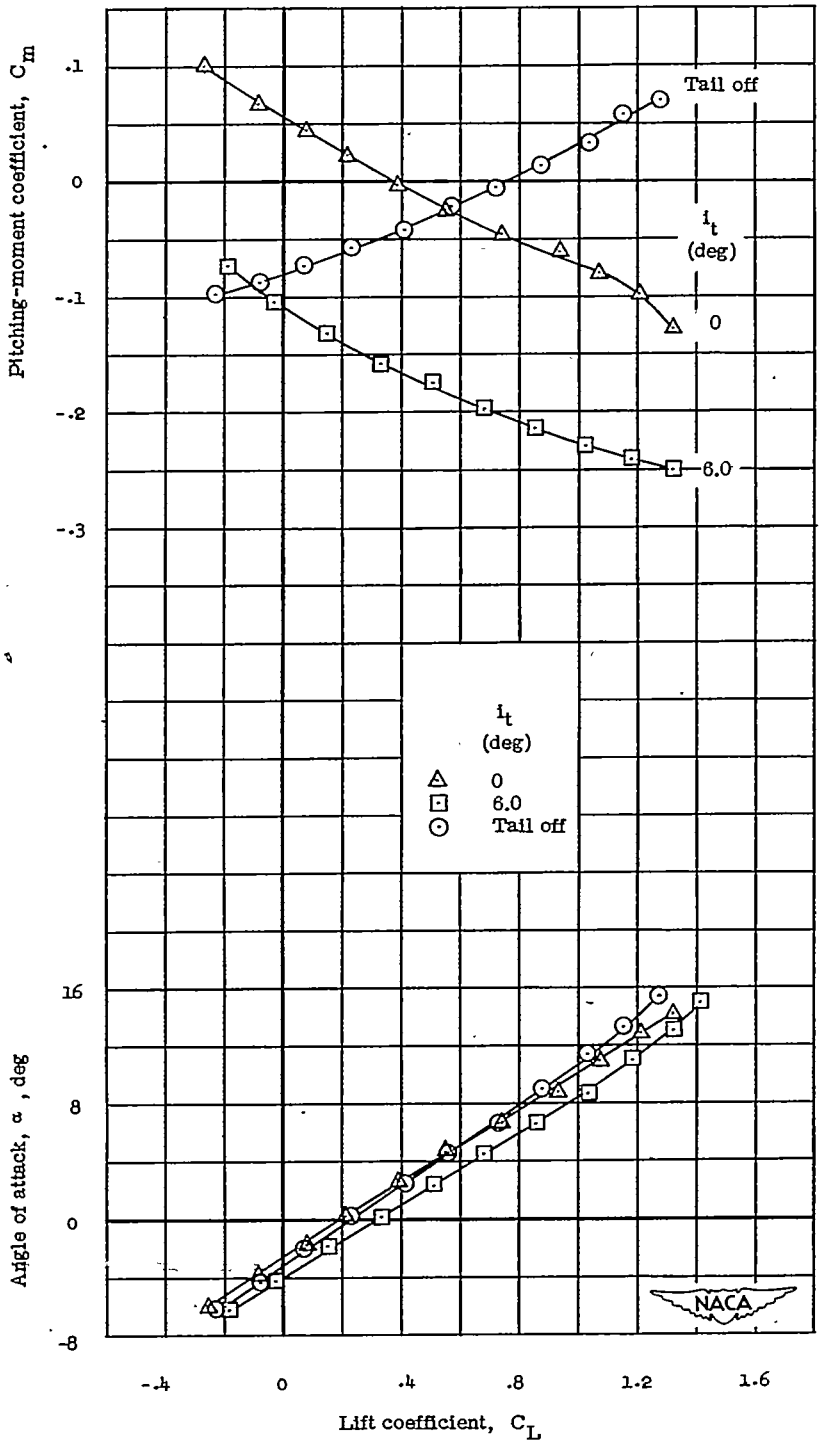

(a) Wind-tunnel data with propeller windmilling.

Figure 12.- Longitudinal characteristics of model 21.

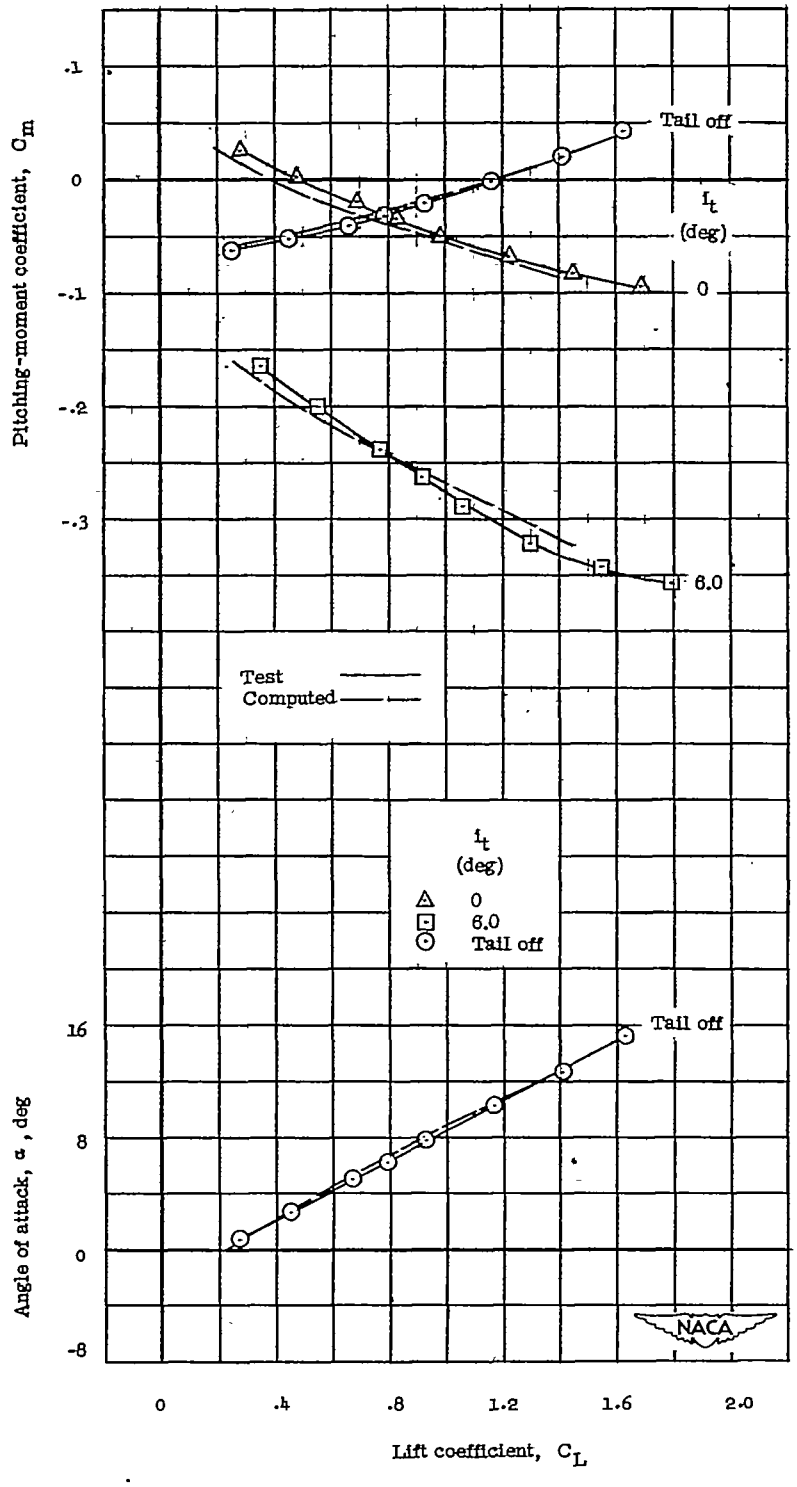

(b) Comparison of computed and experimental data for constant power condition.

Figure 12.- Continued.

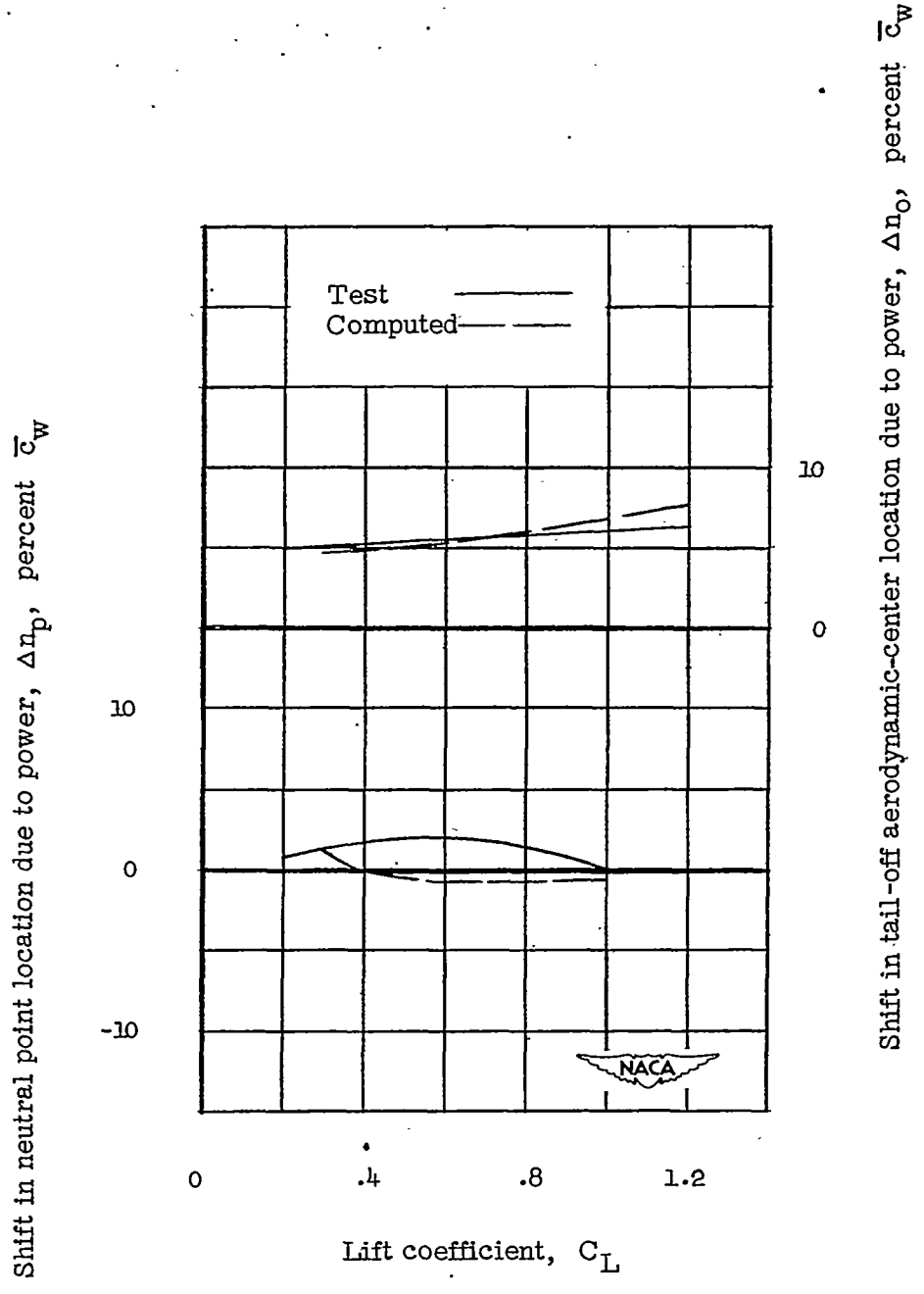

(c) Comparison of computed and experimental effects of power on the neutral point and tail-off aerodynamic-center location.

Figure 12.- Concluded.

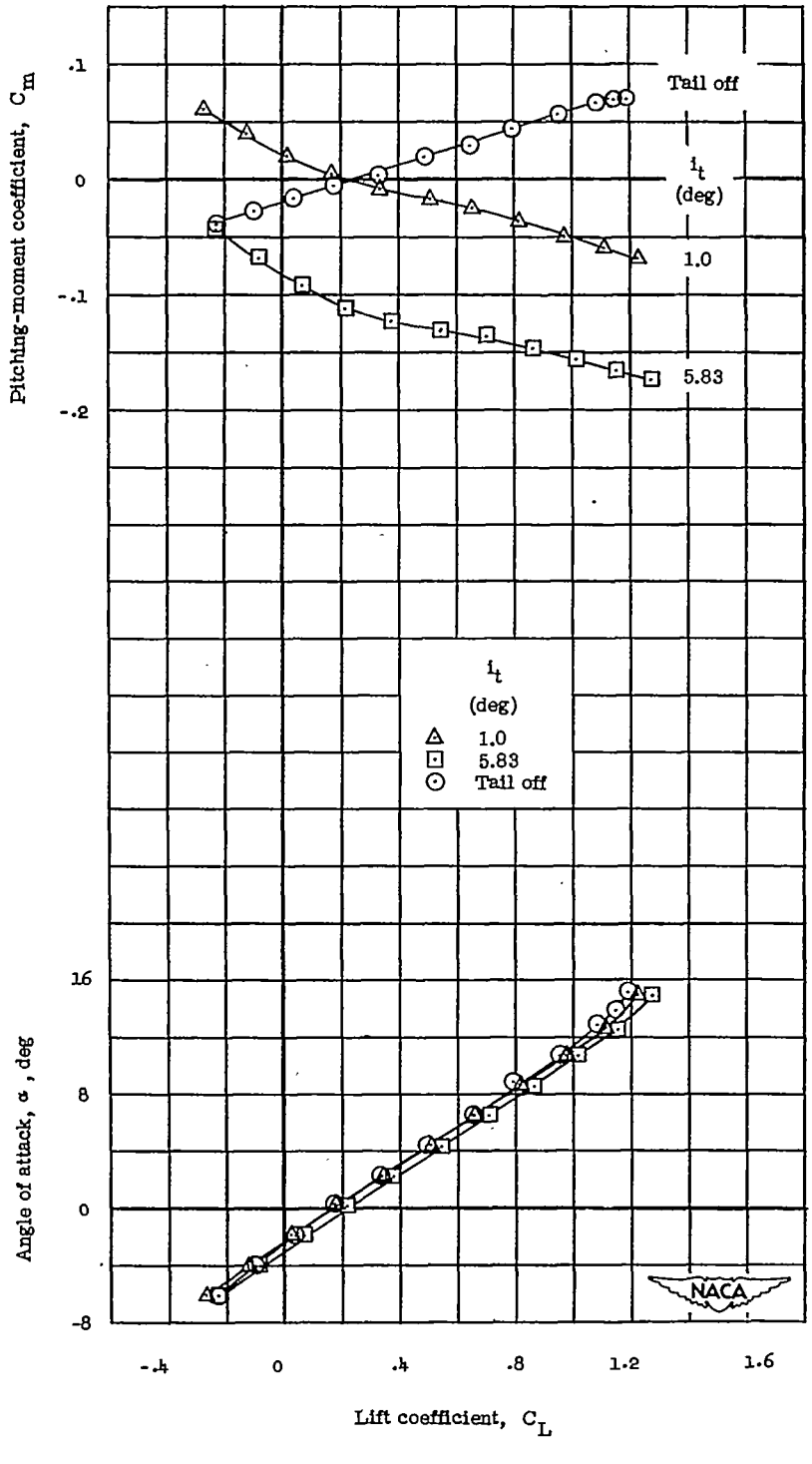

(a) Wind-tunnel data with propeller windmilling.

Figure 13.- Longitudinal characteristics of model 13.

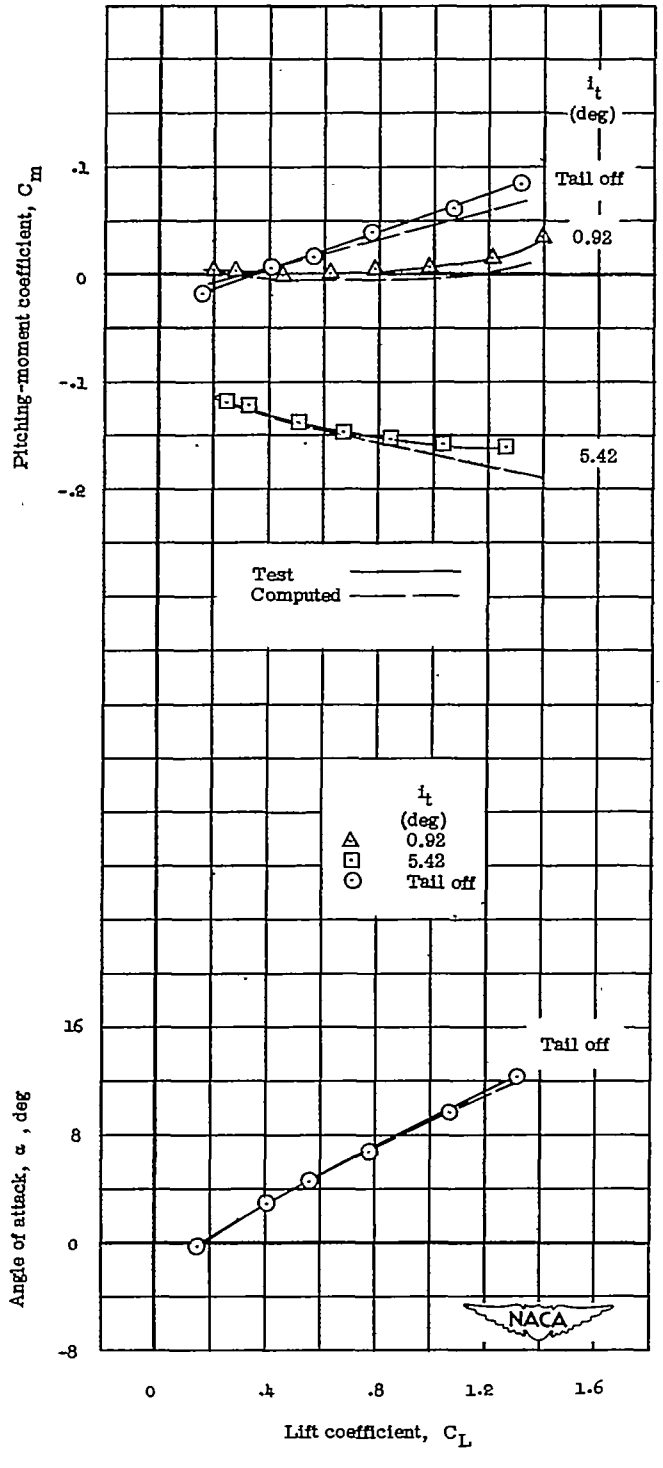

(b) Comparison of computed and experimental data for constant power condition.

Figure 13.- Continued.

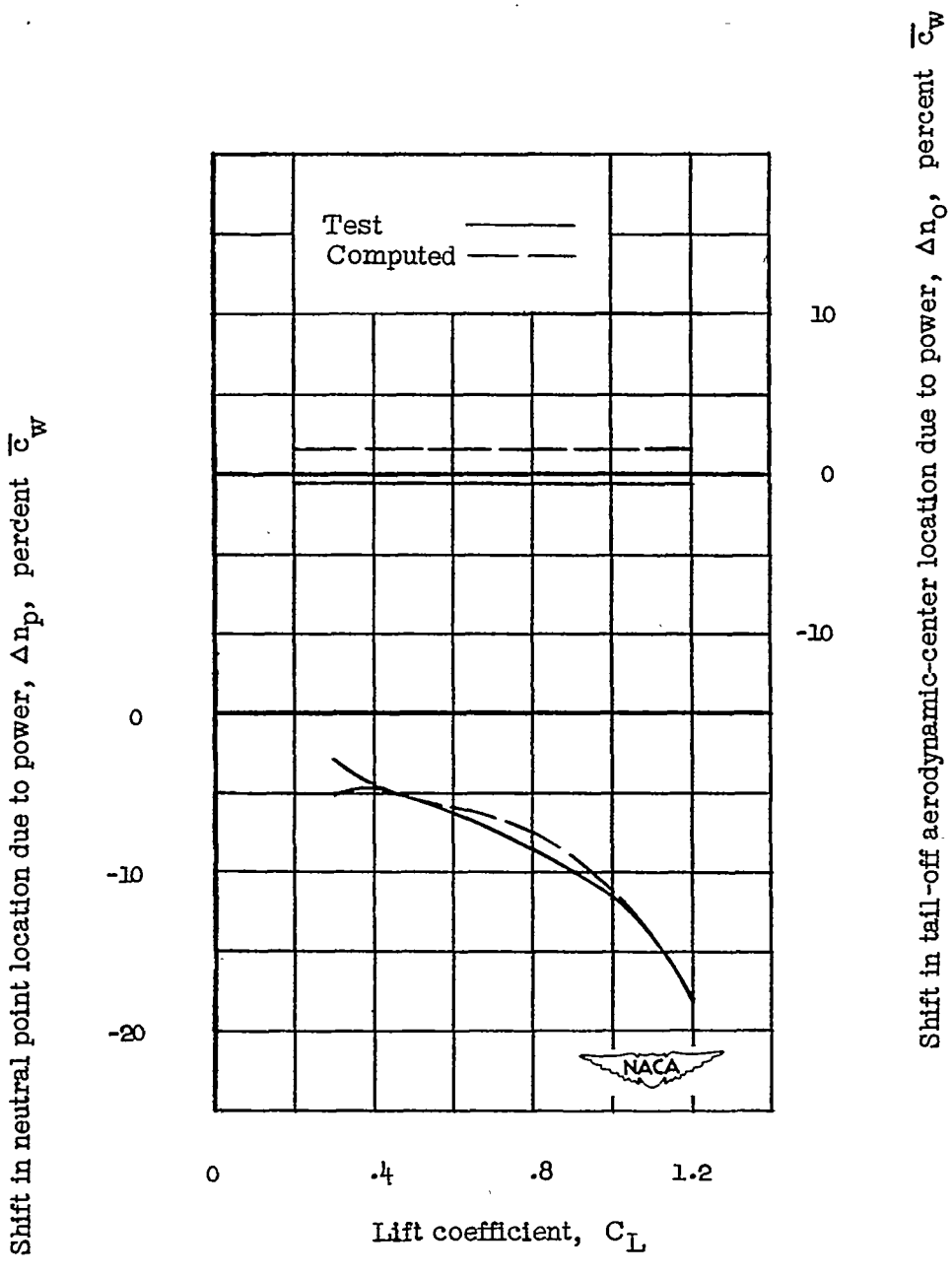

(c) Comparison of computed and experimental effects of power on the neutral point and tail-off aerodynamic center location.

Figure 13.- Concluded.

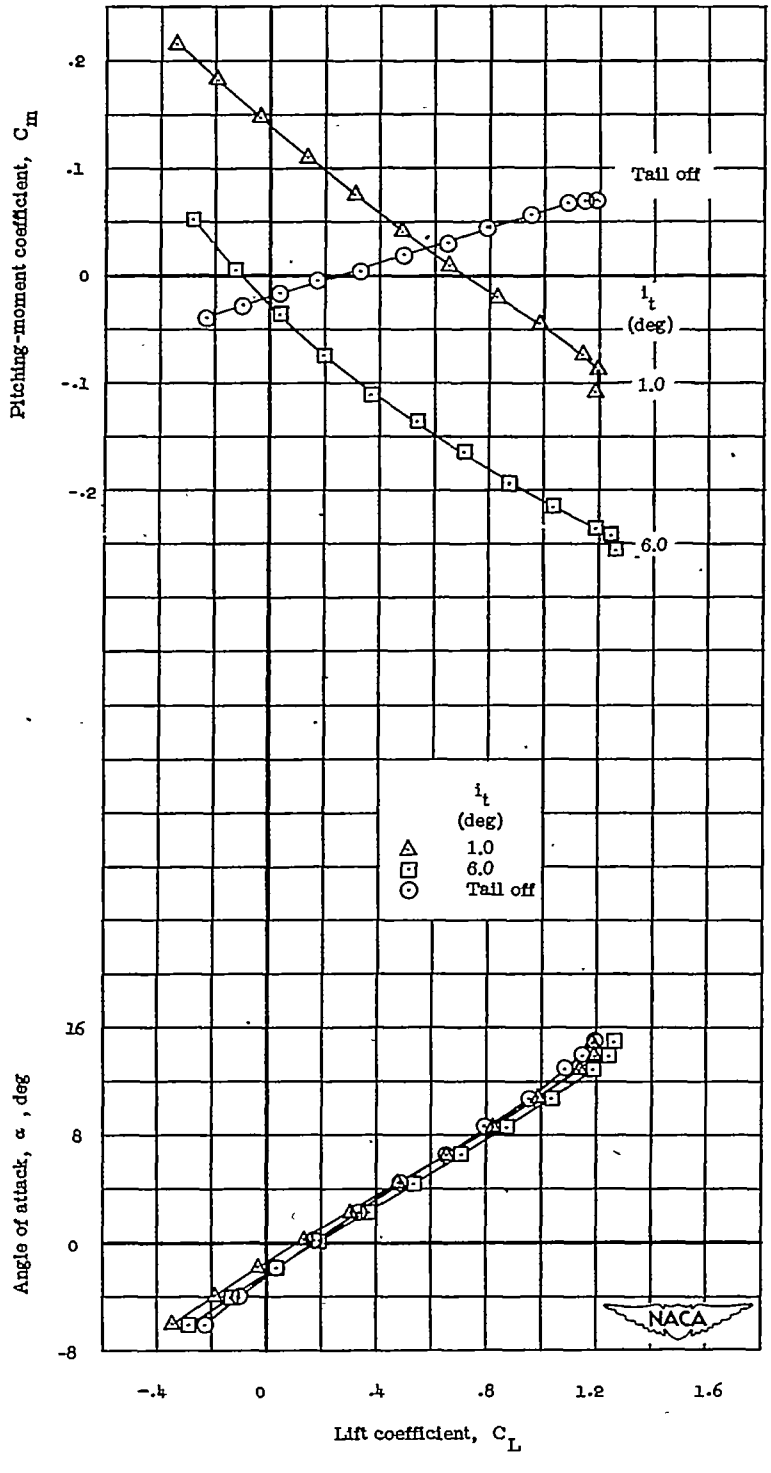

(a) Wind-tunnel data with propeller windmilling.

Figure 14.- Longitudinal characteristics of model 15.

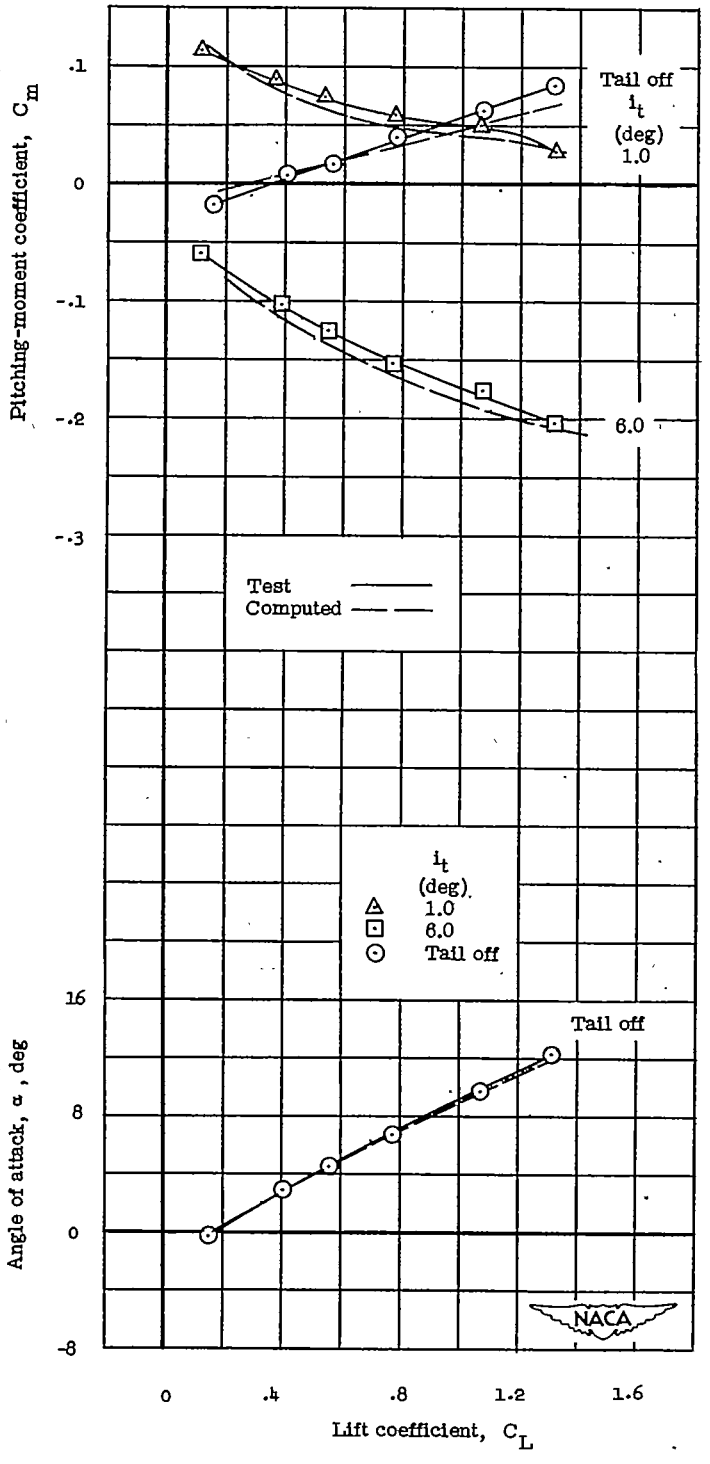

(b) Comparison of computed and experimental data for constant power condition.

Figure 14.- Continued.

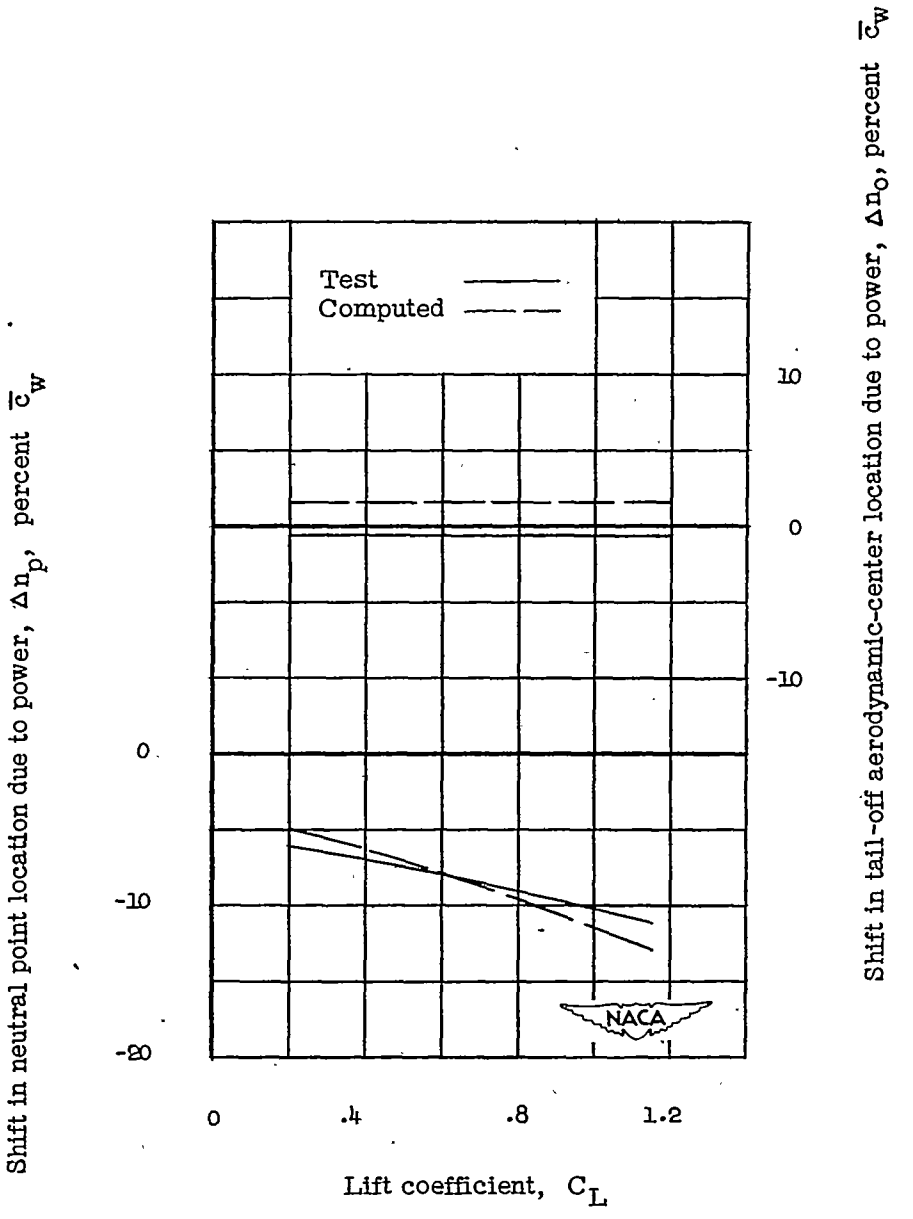

(c) Comparison of computed and experimental effects of power on the neutral point and tail-off aerodynamic-center location.

Figure 14.- Concluded.